2009

Extension of electrical engineering to bioengineering topics: magnetic fermentation and microfluidic nematode assays

Alex John Deutmeyer
Iowa State University

Extension of electrical engineering to bioengineering topics: magnetic fermentation and microfluidic nematode assays

by

Alex John Deutmeyer

A thesis submitted to the graduate faculty

in partial fulfillment of the requirements for the degree of

MASTER OF SCIENCE

Major: Electrical Engineering

Program of Study Committee:
Santosh Pandey, Major Professor
D. Raj Raman
Liang Dong

Iowa State University

Ames, Iowa

2009

TABLE OF CONTENTS

LIST OF TABLES iv

LIST OF FIGURES v

ACKNOWLEDGEMENTS vii

ABSTRACT viii

CHAPTER 1. GENERAL INTRODUCTION 1

CHAPTER 2. MAGNETIC FERMENTATION 2
2.1 Introduction 2
2.1.1 Background 2
2.1.2 Objectives 3
2.1.3 Literature Review 3
2.2 Methods 7
2.2.1 Inoculum Solution 7
2.2.2 Fermentation Medium 8
2.2.3 Magnetic Fermentation Apparatus 9
2.2.4 Fermentation Filtrate Analysis 13
2.2.5 Statistical Analysis 14
2.3 Procedures 14
2.3.1 Spectrophotometer Calibration 14
2.3.2 ATCC 24859® Characterization 15
2.3.3 Magnetic Fermentation 16
2.4 Results and Discussion 17
2.4.1 ATCC® 24859 Characterization 17
2.4.2 2% Dextrose Loading Magnetic Fermentation 20
2.4.3 6% Dextrose Loading Magnetic Fermentation 22
2.5 Conclusions and Future Work 25

CHAPTER 3. MICROFLUIDIC NEMATODE ASSAY 27
3.1 Introduction 27
3.1.1 Background 27
3.1.2 Objectives 28
3.1.3 Literature Review 28
3.1.3.1 Microfluidic Platforms and Microfluidic Nematology 28
3.1.3.2 Nematode Migration and Drug Assays 30
3.2 Methods and Procedures 31
3.2.1 Microfluidic Platform Design and Fabrication 31
3.2.2 Nematode Preparation 35
3.2.3 Data Capture and Analysis 36
3.2.3 Statistical Analysis 40
3.3 Results and Discussion 41
3.3.1 Velocity 41
3.3.2 Amplitude 43
3.3.3 Wavelength 46
3.3.4 Frequency 48

3.3.5 Amplitude/Wavelength Quotient 50
3.4 Conclusions and Future Work 53

CHAPTER 4. GENERAL CONCLUSIONS 55

BIBLIOGRAPHY.....56

LIST OF TABLES

Table 2.1 A partial summary of the methods and results given in the reviewed literature. 7
Table 2.2 *S. cerevisia* ATCC® 24859 cell growth model parameters at starting concentrations from 10^2 to 10^7 CFU/mL. 18
Table 2.3 Cell growth model parameters for 2% dextrose loading magnetic fermentation. .. 21
Table 2.4 Cell growth model parameters for 6% dextrose loading magnetic fermentation. .. 24
Table 3.1 Master mold fabrication steps for 40 µm feature thickness on a 3" silicon wafer. 33
Table 3.2 Microfluidic device fabrication steps. 34

LIST OF FIGURES

Figure 2.1 Homogeneous magnetic field. (A) Magnet placement on flask. Magnetic field contour maps in mT: (B) 0.5 cm from face, (C) in the middle (1.5 cm from face), (D) 2.5 cm from face. 11
Figure 2.2 Non-homogeneous magnetic field. (A) Magnet placement on flask. Magnetic field contour maps in mT: (B) 0.5 cm from face, (C) in the midle (1.5 cm from face), (D) 2.5 cm from face. 11
Figure 2.3 Magnetic fermentation apparatus. 12
Figure 2.4 Shaker with flask locations. 12
Figure 2.5 Spectrophotometer calibration curve. 15
Figure 2.6 Cell growth characterization of *S. cerevisiae* ATCC® 24859. 19
Figure 2.7 Ethanol production characterization of *S. cerevisiae* ATCC® 24859. 19
Figure 2.8 Cell growth for 2% dextrose loading magnetic fermentation. 21
Figure 2.9 Ethanol production for 2% dextrose loading magnetic fermentation. 22
Figure 2.10 Cell growth for 6% dextrose loading magnetic fermentation. 24
Figure 2.11 Ethanol production for 6% dextrose loading magnetic fermentation. 24
Figure 3.1 Microfluidic platform mask layout featuring 300 μm channels. 32
Figure 3.2 Microfluidic channels developed for observation of nematode undulatory parameters. 34
Figure 3.3 Exsheathing of *O. dentatum* with bleach solution. 36
Figure 3.4 Measurement of channel pixel distance and nematode amplitude and wavelength in the MATLAB Image Toolbox. 37
Figure 3.5 Nematode velocity measurement at the initial and final positions. 38
Figure 3.6 Undulatory motion parameters: (A) velocity, (B) amplitude, (C) wavelength. 39
Figure 3.7 Frequency calculation of (A) *O. dentatum* and (B) *H. glycines*. 40
Figure 3.8 Velocity analysis of sheathed *O. dentatum* isolates over three days of experimentation. 42
Figure 3.9 Comparison of the average velocity of *H. glycines* and sheathed, exsheathed, and drugged *O. dentatum*. 42
Figure 3.10 The *O. dentatum* SENS isolate exhibits a significantly larger amplitude than the LEVR isolate. 44
Figure 3.11 Amplitude analysis of sheathed *O. dentatum* isolates over five days of experimentation. 44
Figure 3.12 Comparison of the average amplitude of *H. glycines* and sheathed, exsheathed, and drugged *O. dentatum*. 45
Figure 3.13 Wavelength analysis of sheathed *O. dentatum* isolates over five days of experimentation. 47
Figure 3.14 Comparison of the average wavelength of *H. glycines* and sheathed, exsheathed, and drugged *O. dentatum*. 48
Figure 3.15 Calculated and expected frequencies of *H. glycines* and sheathed, exsheathed, and drugged *O. dentatum*. 49
Figure 3.16 Tangential force exerted by each segment of the nematode body causes forward locomotion. 50

Figure 3.17 A/λ analysis of sheathed *O. dentatum* isolates over five days of experimentation. 51
Figure 3.18 Comparison of the average A/λ of *H. glycines* and sheathed, exsheathed, and drugged *O. dentatum*. 52

ACKNOWLEDGEMENTS

I would like to thank Dr. Santosh Pandey for giving me the opportunity to complete my degree under his guidance, for funding my research, and for providing me with insight that will help me succeed throughout my career. I would like to thank Drs. Pandey, Raj Raman, and Liang Dong for taking time to serve on my committee, and specifically, Dr. Raman for the use of lab space, equipment, and guidance while endeavoring into an entirely new field of research.

Thank you to Patrick Murphy for your mentorship. My progress was immeasurably hastened by the time you took to teach me about the science of fermentation and academic research. Also, thank you for your help with statistical analysis for the fermentation research and obtaining everything that I needed to complete magnetic fermentation research. Thank you to Micky Vincent and Prachand Shrestha for supplying the *S. Cerevisiae* cultures. Thank you to Dr. Richard Martin and Dr. Alan Robertson for supplying me with nematodes, and for meeting with me to discuss research progress and provide guidance. Thank you to Dr. Robertson for helping with the statistical analysis for the nematode research. Thank you to Dr. Thomas Baum for supplying soybean cyst nematodes. Thank you to Baozhen Chen for teaching me fabrication skills and for everything you did to help progress our research.

Thank you to Ben Curtin and Ryan Boesch for your friendship and support throughout our time as undergraduate and graduate Electrical Engineering students.

Finally, I would like to thank my family and friends for always encouraging me to work to the best of my ability.

ABSTRACT

The Department of Electrical and Computer Engineering (ECpE) at Iowa State University added bioengineering to the department's list of strategic research areas in 2006. In an effort to foster a bioengineering center of excellence within the department and to promote multidisciplinary research, two bioengineering research projects were performed: magnetic fermentation and microfluidic nematode assay development. The background of these research topics, the work completed for each, and their future prospects are discussed in this thesis.

Fuel ethanol produced through fermentation has recently received attention during the search for eco-friendly, renewable energy sources. Previous research has been completed to observe the effects of magnetic fermentation but conflicting results have been reported. Research was performed to characterize the fermentation kinetics of *S. Cerevisiae* ATCC® 24859 at cell concentration loading rates from 10^2 to 10^7 CFU/mL and to determine the effects of magnetic field enhanced fermentation on cell growth and ethanol production. It was found that magnetic fields have no statistically significant affect on cell growth. Non-homogeneous static magnetic fields of 220 mT caused a 9% ethanol concentration peak enhancement over the control group for 2% dextrose loading experiments and a peak ethanol concentration six hours before the control group for 6% dextrose loading experiments.

Non-parasitic nematodes are common research subjects, but the characterization of parasitic nematodes has been limited by the versatility and resolution of available technology. A high resolution microfluidic assay for the measurement of parasitic nematodes' undulatory locomotive parameters was developed and tested. A characterization and comparison of these parameters for *H. glycines* and two isolates of *O. dentatum* revealed that a correlation between nematodes' undulatory parameters and their physiological state exists, suggesting prospects for new nematode migration and drug chemotaxis assays.

CHAPTER 1. GENERAL INTRODUCTION

The Department of Electrical and Computer Engineering (ECpE) at Iowa State University has placed increased emphasis on the integration of engineering and life sciences over the past several years. In the 2006 publication of the department's *Research Highlights*, creating a bioengineering center of excellence within ECpE was listed as one of the department's top research priorities. The Department of Electrical and Computer Engineering also added bioengineering to the list of strategic research areas to further encourage professors and students to perform research that will benefit overcoming present and future problems rooted in the biological sciences.

In 2008, a Bioengineering minor was made available to undergraduate engineering students at Iowa State University to help supplement the engineering foundation created through students' major coursework. With the addition of this minor, the College of Engineering has shown support for the ECpE department's efforts to bridge the gap between engineering and life sciences.

With the strategic goals of the ECpE department in mind, bioengineering research was performed to utilize the resources provided by the ECpE department in an effort to foster a bioengineering center of excellence within the department and to promote multidisciplinary research. In the areas of energy, biorenewable resources, and biological systems, the effects of static magnetic fields on the growth of yeast cells and the production of ethanol during fermentation were explored. In the areas of parasitology and biomicro systems, microfluidic platforms were designed, fabricated, and tested to aid in the study and evolution of nematode migration and drug chemotaxis assays. The following thesis individually introduces these research topics, the work completed for each, and their future prospects.

CHAPTER 2. MAGNETIC FERMENTATION

2.1 Introduction

2.1.1 Background

The inevitable depletion of non-renewable energy sources, increased fuel prices, and concern for the environmental effects of burning fossil fuels has created increased demand for the development of eco-friendly, renewable energy sources. One such energy source is fuel ethanol produced through the fermentation of biomass. Fuel ethanol is an attractive renewable energy source because it has net positive energy balance (ratio of energy output to energy input) and because the consumption of carbon dioxide during the growth of biomass offsets fuel ethanol combustion emissions(1). Despite these factors, there are still skeptics of the technology that cite the negative impact that food-based ethanol has had on global food prices(2) and the higher cost of producing fuel ethanol compared to that of typical gasoline(3) as reasons to discontinue widespread use of fuel ethanol. Therefore, the efficiency of ethanol production must be maximized to increase the efficacy of its use as a long-term, renewable energy source.

To aid in this effort, research has been completed to observe the effects of magnetic fields on the yeast cell growth and fermentation of biomass(4)(5)(6)(7)(8)(9)(10). Several of these studies have shown an increase in cellular growth of yeast and/or the production of ethanol(4)(5)(6)(8) while others claim to have seen no effects(9) or negative effects(4)(7)(10). Inconsistencies among these experiments regarding growth medium content, magnetic field strength/type, and fermentation organism and loading rate have made them difficult to compare. This necessitates the conduction of a well-controlled experiment that explores the fermentation kinetics of a common fermentation organism, creating a

baseline for comparison to magnetic fermentation experiments using the same fermentation organism.

2.1.2 Objectives

The objectives of these experiments were to characterize the fermentation kinetics of *S. Cerevisiae* ATCC® 24859 and to determine the effects of externally applied magnetic fields on fermentation by measuring cell growth and ethanol production in a well-controlled experimental system.

2.1.3 Literature Review

There have been several experiments that have observed the effects of magnetic fields on the growth of fermentation organisms and ethanol production. The effects on *S. Cerevisiae* strain DAUFPE-1012 were observed during 24 h magnetic fermentations by Motta et al. (2004). In their experiments, neodymium-iron-boron (NdFeB) rod-shaped magnets were used to produce non-homogeneous magnetic fields with a 220 mT field strength in the middle of a fermentation vessel. The growth medium consisted of 0.5% (w/v) yeast extract and 5% (w/v) glucose. The inoculum added to each fermentation vessel contained approximately $6x10^4$ yeast cells, or approximately 500 cells/mL within 120 mL working volume of yeast suspension. Cellular growth was determined using culture turbidity, the ethanol production level was monitored by gas chromatography, and glucose concentration was evaluated using the dinitrosalicylic acid method. The results of eight separate runs were averaged, yielding standard deviations less than 12% of the mean. Comparing the control group to the experimental groups showed that the glucose consumption rate was 1.3 times higher, the ethanol production rate was 3.4 times higher, and the cellular growth rate was 3.0 times higher in the experimental group. The magnetized experimental group had a higher alcohol per gram of glucose per gram of biomass quotient, indicating magnetic field enhanced ethanol production efficiency.

In a similar experiment, Motta et al. (2001) observed the growth and metabolic activity of *S. Cerevisiae* strain DAUFPE-1012 yeast cultures under 110 mT and 220 mT magnetic fields. A pair of NdFeB magnets were used to produce the 220 mT field strength in the middle a growth flask. A single magnet was used under the flask to produce the field for 110 mT experiments. The growth medium was a 2% glucose medium. Ten percent (v/v) inoculum with cell density ~20,000 cells/mL was added to 10 mL working volume of growth medium. Cellular growth was determined by light spectrophotometry, and carbon dioxide pressure in the growth flask headroom was monitored via a mercury manometer hermetically connected to the growth flask by a polyethylene tube. An initial and final pH value for the culture medium was measured. The resulting absorbance data shows similar cell growth percentage between the control and experimental groups; however, increased carbon dioxide production in the experimental groups suggests altered metabolic activity under magnetic fields.

The effects of extremely low frequency magnetic fields in bioreactor fermentations with *S. Cerevisiae* were observed by Perez et al. (2007). Unlike the previously mentioned experiments, these fermentations were completed in a 5-L BIOFLO-III bioreactor while the cell suspension was recycled through a stainless steel tube, passing the cell suspension through one or two magnetic field apparatuses. The first magnetic field apparatus consisted of six magnets arranged in pairs with opposite poles facing each other and adjustable field strength from 5-20 mT, depending on magnet spacing. The recycling suspension fluid passed through the three fields of alternating polarity, yielding a "low frequency field." The second magnetic field apparatus was a double-layer solenoid, creating an 8 mT field by passing 2 A of current. The growth medium consisted of 16% (w/v) sugar concentration by diluted sugar cane molasses, 0.5% (w/v) KH_2PO_4, 0.12% (w/v) KCl, 0.15% (w/v) NH_4Cl, 0.07% (w/v) $MgSO_4$, and yeast extract. The inoculum cell concentration was not noted in the paper. Sugar concentration in the fermentation medium was determined by the Somogyi-

Nelson method, and the ethanol concentration was monitored by the method used by Salik and Povh. The collected data revealed higher rates of sugar consumption and ethanol production for the experimental magnetic fermentations that were both proportional to the magnetic field strengths. However, the final ethanol concentration was approximately the same among all experiments.

Mehedintu et al. (1997) studied the effects of weak (0.2 mT and 0.5 mT) alternating fields for frequencies between 10 and 100 Hz on the proliferation of yeast. Their fermentation organism was S. Cerevisiae strain H192 ZIMET. Magnetic fields were generated by a pair of Helmholtz coils capable of producing a homogeneous magnetic field strength from 0.1 to 12 mT. The growth medium was a YEPG medium containing 1% (w/v) yeast extract, 2% (w/v) peptone, and 2% (w/v) glucose at a pH 6.5. The inoculation solution had a cell density of approximately 5 – $7x10^6$ cells/mL. Cell growth was monitored by microscopic determinations in a Thoma chamber and Coulter System. Results of fermentations at 0.2 mT, 50 Hz fields showed growth inhibition while fermentation at 0.5 mT, 50 Hz showed growth stimulation. The frequency response between 10 and 100 Hz for field strength of 0.5 mT suggests "windows" of growth stimulation or inhibition. Windows of growth stimulation occurred at 15 Hz and 50 Hz, and windows of inhibition occurred at 10 Hz and 40 Hz when compared to the control.

In contrast, Ruiz-Gomez et al. (2004) saw no effects of static and 50 Hz magnetic fields, strengths 0.35 mT and 2.45 mT, on the growth of *S. Cerevisiae* strain WS8105-1C. Magnetic fields were generated by a pair of Helmholtz coils capable of producing a homogeneous magnetic field strength from 0.1 to 3.5 mT at the middle of the 1.5 mL ependorf tubes used as the growth containers. The growth medium was a YPD broth with 1% (w/v) Bacto-yeast extract, 2% (w/v) Bacto-peptone, and 2% (w/v) dextrose. The inoculation solution had a cell density of approximately 1.13 – $2.24x10^7$ cells/mL. Cell growth was monitored by measuring the optical density of the cell suspension at 600 nm.

Samples taken at 24 and 72 h revealed no statistically significant difference between the control and experimental groups at any of the magnetic field variations tested.

The effects of strong static magnetic fields on the proliferation of yeast were observed by Iwasaka et al. (2004). An unspecified strain of *S. Cerevisiae* was used for these experiments. Magnetic fields were generated by a superconducting magnet capable of producing field strengths up to 14 T. The growth medium was a peptone-glucose medium of 0.4% (w/v) peptone and 2% (w/v) glucose. The cell density of the inoculation solution was not specified; however, the optical density of the initial yeast suspension was 0.4 at a wavelength of 600 nm. Cell growth was monitored by measuring the optical density of the cell suspension at 600 nm. Optical density data for a control group and an experimental group under a 14 T static magnetic field was collected. From this data, the differential optical density was obtained by subtracting the optical density of the experimental group from the optical density of the control group. A trend of moderately delayed proliferation under strong static magnetic fields was found after experimentation.

Cell proliferation under strong static magnetic fields was also observed by Ostabe et al. (2009). Two different fermentation organisms were used in their experiments, including *S. Cerevisiae* strains K-7 and W303-1a. *S. Cerevisiae* strain W303-1a was used in the experiments pertinent to this thesis. Magnetic fields were generated by a superconducting magnet capable of producing field strengths up to 10 T. The growth medium was a YPD medium containing 1% (w/v) yeast extract, 2% (w/v) peptone and 2% (w/v) dextrose. The cell density of the inoculation solution was approximately $5x10^6$ cells/mL. Cell growth was monitored by a standard plate count technique. Magnetic cell growth experiments under static magnetic fields of 0, 1, 3, 5, 7, and 10 T resulted in moderate inhibition of cell growth. These results appear to be in accordance with those found by Iwasaka et al. (2004).

A partial summary of the methods and results from the reviewed literature may be found in Table 2.1. This summary demonstrates the variability of magnetic experiments in

yeast strain, organism loading rate, magnetic field type, and results. The variability in organism loading rate inspired the characterization of the fermentation kinetics for various organism loading rates, and the positive results of Motta et al. (2001, 2004) influenced the use of magnetic fields on the order of hundreds of milliTeslas for this research. A common sugar loading rate of 2% (w/v) was present.

Table 2.1 A partial summary of the methods and results given in the reviewed literature.

Source	*S. cerevisiae* strain	Organism loading rate (cells/mL)	Sugar loading rate (w/v)	Magnetic field	Experimental results
Motta 2004	DAUFPE-1012	500	2%	220 mT, SMF	Cell growth, EtOH prod., and glucose consumption rates increase
Motta 2001	DAUFPE-1012	2×10^4	2%	110 mT, 220 mT, SMF	CO_2 production increase
Perez 2007	-	-	16%	5-20 mT, solenoid, ELF	EtOH prod. rate increase
Mehedintu 1997	H192 Zimet	$5\text{-}7 \times 10^6$	2%	0.5 mT, 10-100 Hz	Various cell growth increase and inhibition
Ruiz-Gomez 2004	WS8105-1C	$1\text{-}2 \times 10^7$	2%	0.35 mT, 2.45 mT, SMF, 50 Hz	No effects
Iwasaka 2004	-	-	2%	14 T, SMF	Cell growth inhibition
Ostabe 2009	W303-1a	5×10^6	2%	0-10 T, SMF	Cell growth inhibition

2.2 Methods

2.2.1 Inoculum Solution

Experiments were completed with *Saccharomyces Cerevisiae* strain ATCC® 24859. This wild-type diploid strain was chosen because it has been shown to possess high ethanol

concentration tolerance(11). An initial cell growth was completed followed by refrigeration in 2 mL cryogenic vials at -80˚C.

Inoculum solution was prepared prior to each fermentation experiment by aseptically adding the contents of one cryogenic vial to 150 mL working volume of culture broth containing 10% (v/v) 10X YP medium prepared according to NREL protocol(12), 2% (w/v) dextrose, 5% (v/v) 1.0 M citrate buffer prepared according to NREL protocol(12), pre-sterilized by autoclaving at 121˚C for 20 min., in a 250 mL DeLong fermentation flask with aluminum closure (Bellco Glass, Vineland, NJ). The solution was vortexed and incubated at 35˚C for 24 h in a shaking water bath (New Brunswick Scientific, Edison, NJ) at 150 rpm.

2.2.2 Fermentation Medium

The fermentation medium contained 10% (v/v) 10X YP medium and 5% (v/v) 1.0 M citrate buffer, both prepared according to NREL protocol(12). In order to test the dependence of the magnetic fermentation effects on fermentation medium sugar concentration, two different dextrose loading rates were chosen for the magnetic fermentation experiments. The “low” loading fermentation medium contained 2% (w/v) dextrose while the “high” loading fermentation medium contained 6% (w/v) dextrose.

Autoclaving for fermentation medium sterilization presents the risk of caramelizing sugars in a growth solution(13). To prevent excessive destruction of sugars within the 6% dextrose loaded fermentation medium, it was autoclaved prior to the addition of dextrose. A 30% (w/v) dextrose solution was mixed during fermentation preparation and sterilized by filtration through a 200 nm filter via syringe. It was then aseptically added to the pre-sterilized fermentation medium at a dilution rate necessary to achieve a final high loading fermentation medium with a dextrose concentration of 6%.

2.2.3 Magnetic Fermentation Apparatus

Initial trials with magnetic fermentation demonstrated the difficulties in using typical fermentation equipment with permanent magnets. The sloped sides of DeLong fermentation flasks provided unstable resting places for the powerful magnets used in these experiments. The wide base of the flasks also created a large radius between the two magnetic poles. The force between two magnetic poles is inversely proportional to the radius squared:

$$F = \frac{\mu m_1 m_2}{4\pi r^2}$$

The relatively large base diameter of the DeLong fermentation flask reduces the maximum magnetic force at the center of the yeast suspension so a fermentation vessel with a minimal base width and a sufficient volume is desirable. BD Falcon 250 mL tissue culture flasks (BD Biosciences, Bedford, MA) were chosen as the fermentation vessels to overcome both of these obstacles. Tissue culture flasks have flat, parallel sides, so the force between magnetic poles securely holds them in place without risking accidental magnet convergence. Tissue culture flasks also have relatively small widths for moderate container volumes because they are designed for maximum flat area, enabling large magnetic fields to be produced with commercially available permanent magnets.

Magnetic fields for the experimental groups were generated by ultra-high-pull neodymium-iron-boron magnets. The first magnetic field was a homogeneous (single magnetic dipole), static magnetic field (HMF) produced by two 3” dia. x 0.25” thick, non-plated disc magnets with 50 lbs. of pull force (McMaster-Carr, Elmhurst, IL). The second magnetic field was a non-homogeneous (multiple magnetic dipoles), static magnetic field (NHMF) produced by eight 1” dia. x 0.5” thick, nickel plated disc magnets with 38 lbs. of pull force (McMaster-Carr). With the magnets in place on the sides of tissue culture flasks as shown in Figures 2.1a and 2.2a, the magnetic field strengths of both the homogeneous and non-homogeneous fields were measured. A Lake Shore Model 410 handheld gaussmeter

with an accuracy of ±2% and a Lake Shore Model 410 transverse probe (Lake Shore Cryotronics Inc., Westerville, OH) were used to measure field strength at 216 evenly spaced sampling points within the tissue culture flask: 8 along the length by 9 along the height by 3 along the width. The magnitude of the homogeneous field in the middle of the two 3" magnets varied from 115 to 130 mT. The magnitude of the non-homogeneous field in the middle of the 1" magnets varied from 80 to 200 mT. Contour maps of the homogeneous magnetic field strength in milliTeslas may be seen in Figure 2.1b-d. A nearly uniform field is present for a large volume between the two magnetic poles. Similar contour maps of the non-homogeneous magnetic field strength in milliTeslas may be seen in Figure 2.2b-d. Here, four pairs of magnetic poles create two different magnetic field polarities. The non-homogeneous field also has much more variation in field strength from the edge of the flask to the middle. These fields were designed to reveal if maximum field strength or maximum field volume would create a greater change in the fermentation kinetics.

The shaking water bath used for inoculum preparation is made with stainless steel which could interfere with the magnetic fields used in the magnetic fermentation experiments. Water immersion could also lead to damage of the non-plated magnets. A Model 307C Fisher Scientific low temperature incubator (Fisher Scientific, Fair Lawn, NY) housed two Innova 2000 shaker stages (New Brunswick Scientific) for magnetic fermentation experiments. Shaker tables were equipped with metal racks and bungee cords to securely hold all flasks in place during fermentations. The metal rack was found to interfere with the magnetic fields; as a result, 0.5" thick sheets of plywood were cut and placed inside each rack. The magnetic fields inside each flask were measured in this setup and were found to be negligibly different than as described above. The magnetic fields in the control

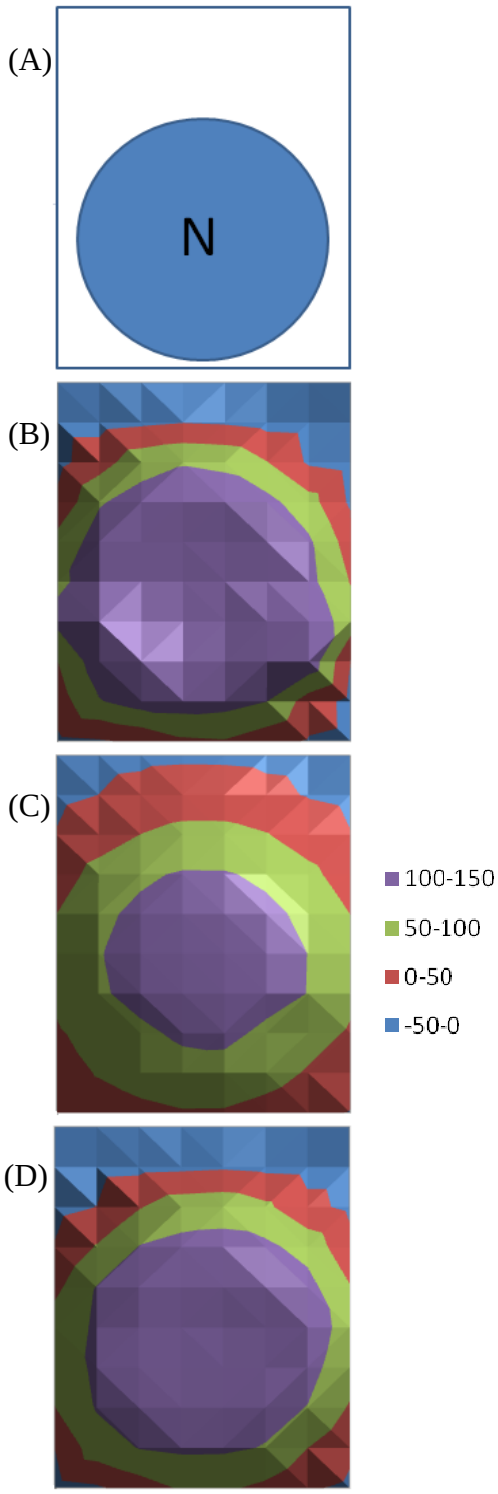

Figure 2.1 Homogeneous magnetic field. (A) Magnet placement on flask. Magnetic field contour maps in mT: (B) 0.5 cm from face, (C) in the middle (1.5 cm from face), (D) 2.5 cm from face.

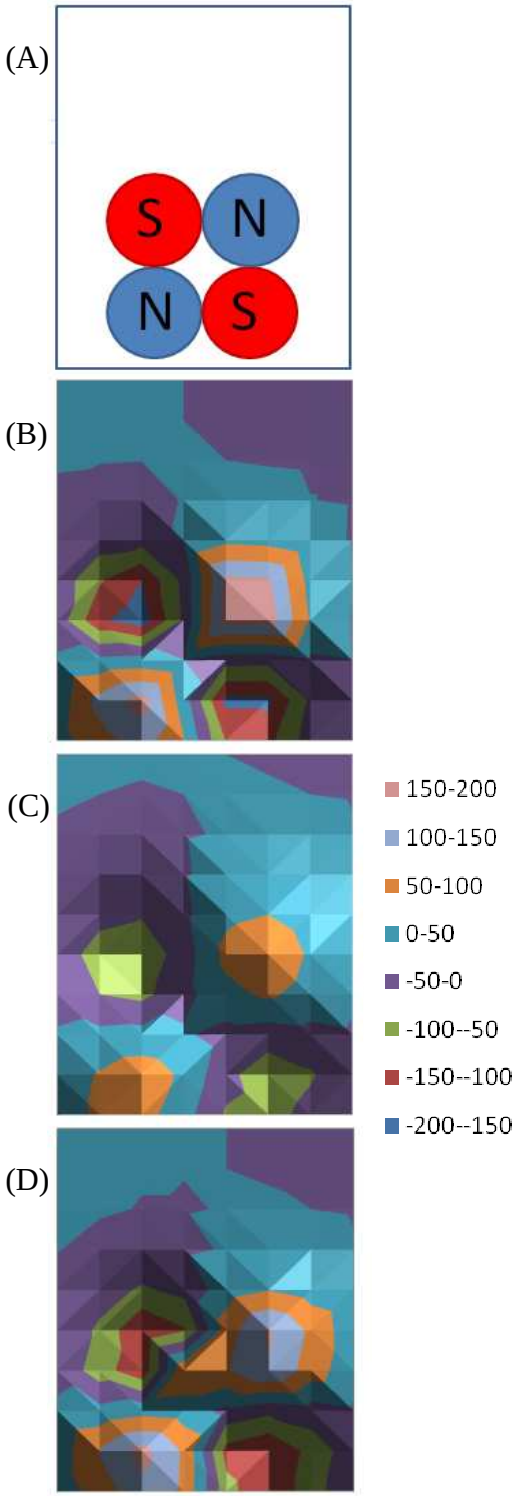

Figure 2.2 Non-homogeneous magnetic field. (A) Magnet placement on flask. Magnetic field contour maps in mT: (B) 0.5 cm from face, (C) in the midle (1.5 cm from face), (D) 2.5 cm from face.

flasks were also measured and found to contain a negligible magnetic field strength. The apparatus may be seen in Figure 2.3 and the flask locations Figure 2.4.

Figure 2.3 Magnetic fermentation apparatus.

Figure 2.4 Shaker with flask locations.

2.2.4 Fermentation Filtrate Analysis

For these experiments, the yeast cell growth and ethanol production characteristics of the fermentation are of particular interest. Yeast cell density, also known as colony forming unit (CFU) density, was determined by one of two methods. For cell densities greater than approximately 10^5 CFU/mL, the optical absorption of the cell suspension at 600 nm was measured. A Genesys 6 spectrophotometer (Thermo Electron Corp., Waltham, MA) was used to measure the optical absorption of cell suspensions at 600 nm. The optical absorption was then related to the CFU density by the following equation

$$Density = 2.046 \times 10^7 \cdot Absorption^2 + 1.246 \times 10^7 \cdot Absorption + 3.5841 \times 10^4$$

which was determined by spectrophotometer calibration as described in section 2.3.1 of this thesis. For densities above approximately 10^8 CFU/mL, the optical absorption of the spectrophotometer was saturated so the cell suspension must first be appropriately diluted to avoid saturation. After the cell density of the diluted suspension was determined by the previously mentioned method, it was be multiplied by the amount of dilution to yield the final cell density.

For cell suspensions with cell densities that were below the sensitivity of the spectrophotometer, there was no optical absorption. To determine these lower cell densities, 0.1 mL of solution was plated on sterile YPD agar plates which were prepared according to NREL protocol(12). These plates were incubated at 35˚C until visible colonies were formed. CFU density was then determined by a hand count of colonies.

Fermentation filtrates were analyzed for ethanol by high-performance liquid chromatography (HPLC). The HPLC system consisted of a Varian Prostar 355 refractive index detector (Varian, Palo Alto, CA), a Bio Rad ethanol column (Bio Rad Laboratories, Hercules, CA), Model 400 auto sampler (Varian), and Prostar Model 510 column oven (Varian). Separations were made using 0.01 N sulfuric acid as the mobile phase at a flow

rate of 0.6 mL min^{-1}, a column temperature of 65˚C, and an injection volume of 20 µL. Ethanol standards of 30, 15, 7.5, and 3.75 g/L were used for HPLC calibration based on peak area for each ethanol density.

2.2.5 Statistical Analysis

The fermentation trials were conducted using a randomized complete block design with four replications. Statistical analysis was completed using SAS software. Trends in cell growth data were fit with a logistic growth model found in (14). The significance of the effects of magnetic field, time, and their interaction on ethanol yield was determined using the general linear model procedure. All comparisons were determined to be significant at $p < 0.05$.

2.3 Procedures

2.3.1 Spectrophotometer Calibration

To hasten the process of determining CFU density of yeast cells during fermentation experiments, measurement of the optical absorption was used for densities greater than approximately 10^5 CFU/mL. In order for the optical absorption of a solution to be related to the cell density, spectrophotometer calibration must be performed(15).

Calibration was initiated by preparing 150 mL of inoculum solution as described in section 2.2.1 and 100 mL of fermentation medium without yeast cells as described in section 2.2.2. Inoculum solution was expected to have about 10^8 CFU/mL, so seven serial dilutions were performed to yield suspensions with approximately 10 – 10^8 CFU/mL. Serial dilution of the fermentation medium was also performed. The optical absorption of each inoculum solution and fermentation medium dilution at 600 nm was then measured with a spectrophotometer. 0.1 mL of each cell suspension dilution was plated on three YPD agar plates and incubated at 35˚C until visible colonies were formed. Only the ~10^1 and ~10^2

CFU/mL solutions had sufficient spacing between colonies to enable hand counting. Of these two, the standard deviation/mean quotient of the three ~10^2 CFU/mL counts was much smaller so the average CFU count of the ~10^2 CFU/mL plates was obtained and extrapolated to an order of 10^8 CFU/mL. The optical absorption of the fermentation medium was then subtracted from the optical absorption of the inoculum solution to yield the optical absorption of only the suspended cells. Two repetitions of this process were completed to ensure correct calibration. The absorption data was plotted versus the extrapolated CFU densities obtained from the plate counts. As shown in Figure 2.5, a second order curve was fit to the data points to obtain a calibration curve for translating optical absorption of the cell suspension to cell density.

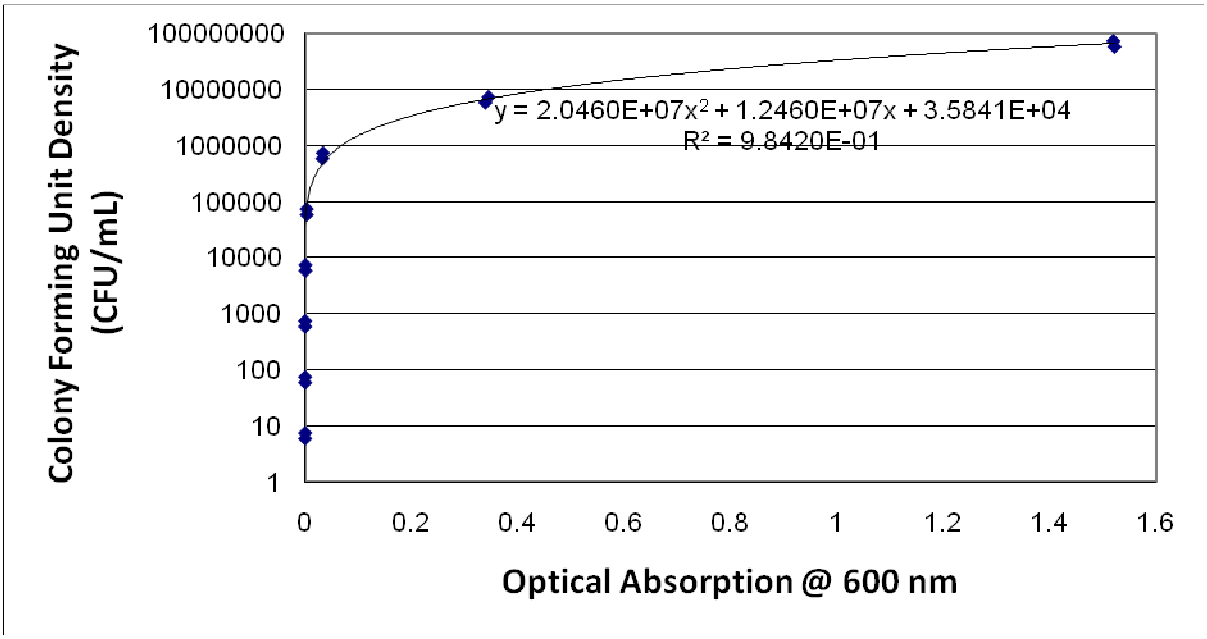

Figure 2.5 Spectrophotometer calibration curve.

2.3.2 ATCC 24859® Characterization

Characterization experiments were initiated by preparing 150 mL of inoculum solution as described in section 2.2.1 and eighteen 150 mL DeLong fermentation flasks with aluminum closures (Bellco Glass), each containing 90 mL of 2% dextrose loaded

fermentation medium as described in section 2.2.2. The inoculum was serially diluted at a 10:1 ratio five times to obtain six evenly spaced starting inoculum densities on a log scale. The eighteen 150 mL fermentation flasks were separated into three repetitions. Each flask was aseptically inoculated with 10 mL from one of the six inoculum densities. The eighteen fermentation flasks were vortexed and incubated at 35˚C for 72 h in a shaking water bath (New Brunswick Scientific) at 150 rpm. 5 mL samples were collected at hours 0, 4, 12, 24, 48, and 72. These filtrates were analyzed as described in section 2.2.4 to yield the results found in section 2.4.1.

2.3.3 Magnetic Fermentation

Magnetic fermentation experiments were initiated by preparing 150 mL of inoculum solution as described in section 2.2.1 and the appropriate number of 150 mL DeLong fermentation flasks with aluminum closures (Bellco Glass), each containing 90 mL of either 2% or 6% dextrose loaded fermentation medium as described in section 2.2.2. The inoculum was serially diluted to a density on the order of 10^4 CFU/mL. Heat transfer occurs more slowly in a dry fermentation apparatus, as described in section 2.2.3, so the fermentation medium, tissue culture flasks, and magnets were all preheated to 35˚C prior to inoculation. The contents of the 150 mL DeLong fermentation flasks were transferred to tissue culture flasks. Each tissue culture flask was aseptically inoculated with 10 mL of the diluted inoculum solution to obtain an approximate starting density on the order of 10^3 CFU/mL. The tissue culture flasks have a standard plug cap that does not allow airflow into the flask; therefore, the flasks were covered with a porous lid to enable aeration and aluminum foil to prevent contamination. The tissue culture flasks were vortexed and incubated at 35˚C at 115 rpm. The rectangular shape of the tissue culture flasks created an unacceptable amount of sloshing at higher vortex speeds, preventing the use of 150 rpm as was used in the growth characterization experiments. The fermentation kinetics of ATCC® 24859 are different at

the low and high sugar loading rates used in these experiments. At 2% dextrose loading rate, the total fermentation time was 25 h with 4 mL samples collected at hours 0, 5, 10, 15, 20, and 25. At 6% loading rate, the total fermentation time was 30 h with 4 mL samples collected at hours 0, 6, 12, 18, 24, and 30. These filtrates were analyzed as described in section 2.2.4 to yield the results found in sections 2.4.2 and 2.4.3.

2.4 Results and Discussion

2.4.1 ATCC® 24859 Characterization

In this section, the results are given for the ATCC® 24859 fermentation kinetics characterization experiments. Cell growth was modeled by the logistic growth model found in (14) which is of the form

$$X = \frac{X_0 e^{kt}}{1 - \frac{X_0}{X_\infty}(1 - e^{kt})}$$

The parameter X_0 was fixed to the average measured starting cell concentration of each data set to increase the accuracy of the models at time 0 h. The model parameters for all cell concentrations may be found in Table 2.2. A plot of cell growth data and cell growth models versus time for all starting cell concentrations may be seen in Figure 2.6. A plot of ethanol production versus time for all starting cell concentrations may be seen in Figure 2.7. Though these experiments were conducted for 72 h, the results clearly show that both cell growth and ethanol production were completed within 24 to 30 h for all starting cell concentrations. As expected, cell growth showed a logistic growth pattern; however, the growth rate of the higher starting concentrations was immediately inhibited due to high cell density. There was a notable lag time in ethanol production for all starting cell concentrations below 10^6 CFU/mL. The maximum ethanol yield was 81.9%, 84.7%, 80.2%, 84.6%, 83.9%, and 83.2% of the theoretical yield for starting concentrations of 10^7, 10^6, 10^5, 10^4, 10^3, and 10^2 CFU/mL, respectively.

Table 2.2 *S. cerevisia* ATCC® 24859 cell growth model parameters at starting concentrations from 10^2 to 10^7 CFU/mL.

Starting Concentration (CFU/mL)	X_0	X_∞	k
10^7	6,100,000	77 x10^6	0.25
10^6	460,000	72 x10^6	0.41
10^5	64,000	72 x10^6	0.67
10^4	6,400	71 x10^6	0.60
10^3	790	75 x10^6	0.53
10^2	110	76 x10^6	0.63

The goal of the magnetic fermentation experiments is to determine the effects of magnetic field enhanced fermentation on cell growth and ethanol production. It was hypothesized that this enhancement could result in a decrease in ethanol production lag time, making it necessary to choose a starting concentration low enough to exhibit ethanol production lag. It was also hypothesized that the enhancement could result in an increase in the CFU growth rate, model parameter k, making it also necessary to choose a starting concentration that exhibits logistic growth over a large time window. Both of these traits were demonstrated by the results of the 10^3 CFU/mL starting concentration data so it was chosen as the starting cell concentration for the magnetic fermentation experiments.

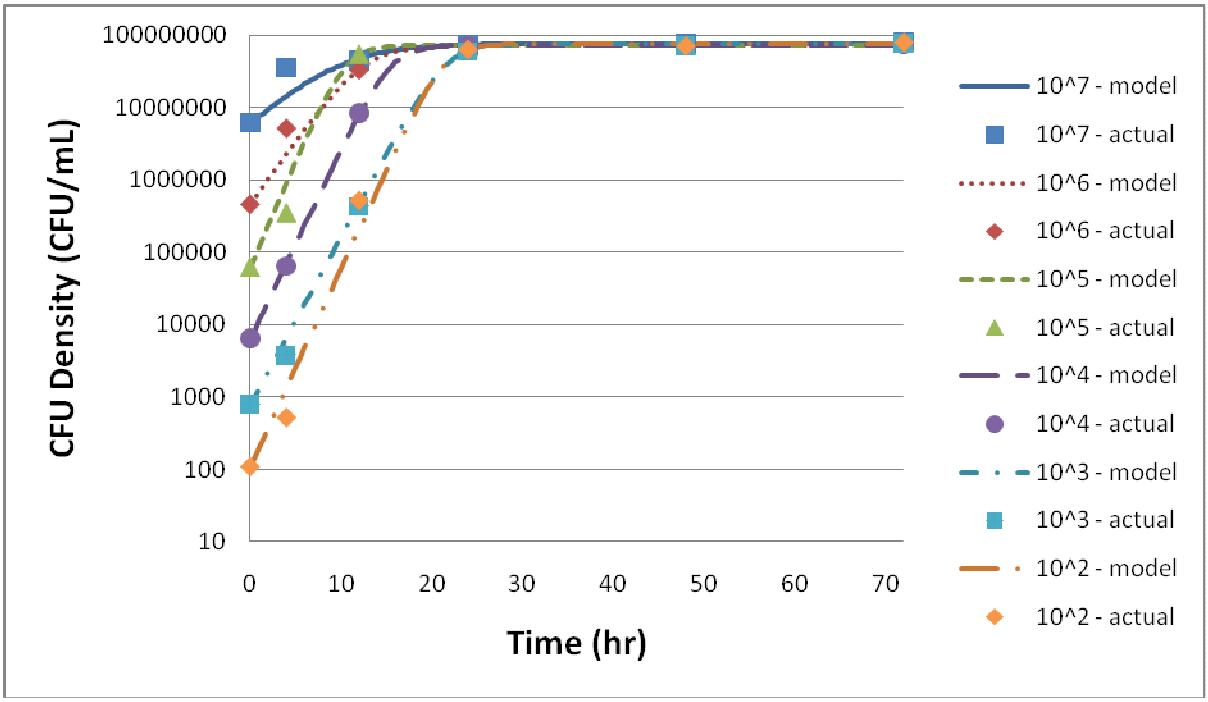

Figure 2.6 Cell growth characterization of *S. cerevisiae* ATCC® 24859.

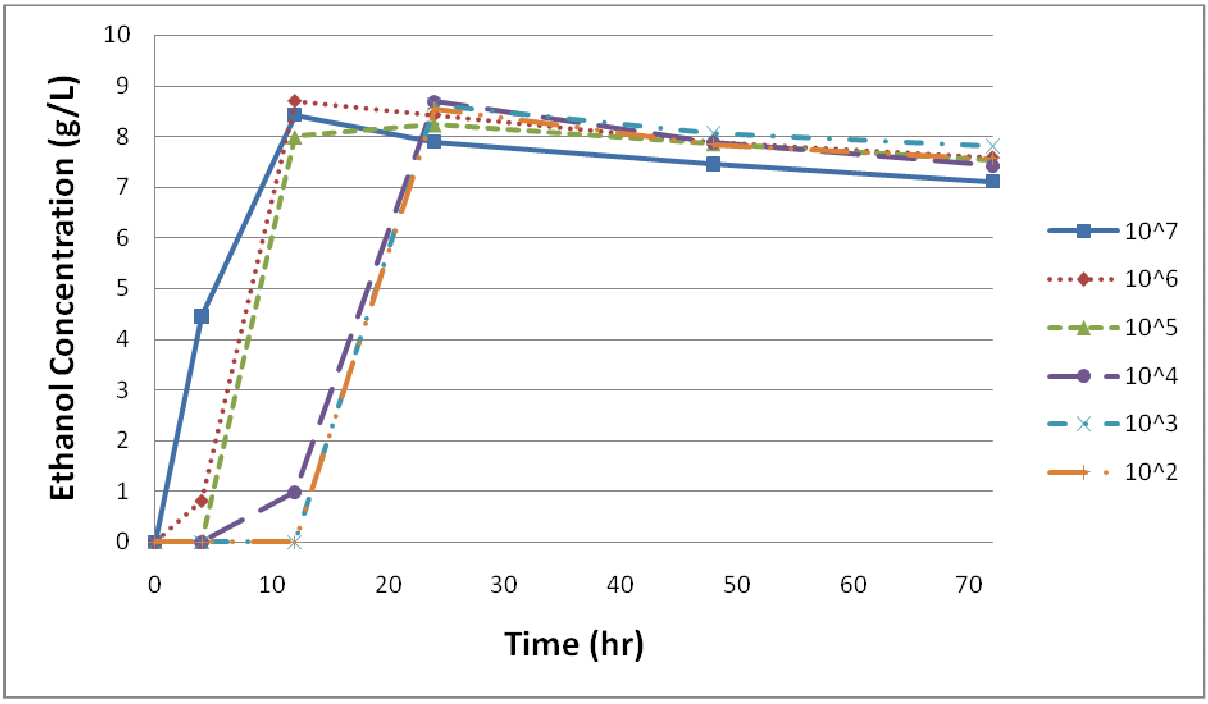

Figure 2.7 Ethanol production characterization of *S. cerevisiae* ATCC® 24859.

2.4.2 2% Dextrose Loading Magnetic Fermentation

In this section, the results are given for the 2% dextrose loading rate magnetic experiments. A plot of cell growth data and growth models versus time for the control and experimental groups may be seen in Figure 2.8. A plot of ethanol production versus time for all groups may be seen in Figure 2.9. Cell growth was modeled with the previously mentioned logistic growth model; the model parameters for all data sets may be seen in Table 2.3.

The plots shown in Figure 2.8 suggest no difference between the cell growth of the control group and experimental groups, both in terms of growth rate and final CFU concentration. Statistical analysis of the model parameters confirmed this observation. These results are in contrast to those reported in (5) and (6) where both homogeneous and non-homogeneous static magnetic fields on the order of hundreds of mT produced significant differences in cell growth when compared to a control group under no magnetic field.

Figure 2.9 shows ethanol production beginning sometime between hours 10 and 15 for all groups, after the CFU density surpasses approximately 10^5 CFU/mL. The peaks in ethanol concentration at hour 20 were used to calculate ethanol yields of 86.9%, 86.6%, and 94.6% of the theoretical yield for the control, HMF, and NHMF groups, respectively. A peak enhancement of approximately 9% was calculated for the NHMF group versus the control and HMF groups. These ethanol yields suggested a significant difference between the NHMF group and the control and HMF groups. Statistical analysis of the ethanol data using the general linear model procedure confirmed a statistically significant difference between the ethanol production of the NHMF group and both the control and HMF groups with a P-value of 0.0086. However, there was no significant difference between the HMF group and the control group.

The ethanol production results create several interesting scenarios. One scenario is that non-homogeneous static magnetic fields promote ethanol production enhancement while

homogeneous static magnetic fields do not. This case partially supports the enhanced ethanol production reported by Motta et al. (2004) and Perez et al. (2007) in the presence of non-homogeneous static magnetic fields of 220 mT and 5 or 20 mT, respectively. However, Motta et al. (2004) also reported magnetically enhanced cell growth which contradicts the results of this experiment. Another scenario is that ethanol production enhancement is a function of magnetic field strength; however, there are no reports of a thorough characterization of this relationship, which means there is no supporting evidence for this case.

Table 2.3 Cell growth model parameters for 2% dextrose loading magnetic fermentation.

Set	X_0	X_∞	k
Control	720	74×10^6	0.65
HMF	720	74×10^6	0.65
NHMF	720	75×10^6	0.65

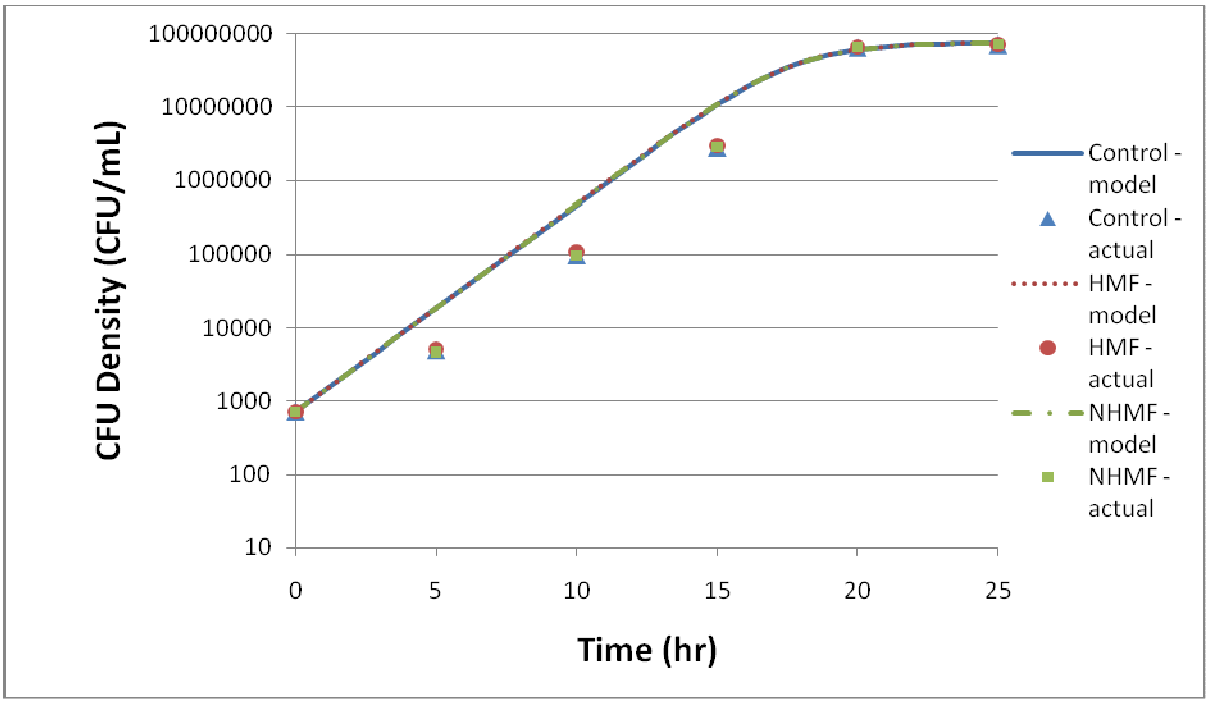

Figure 2.8 Cell growth for 2% dextrose loading magnetic fermentation.

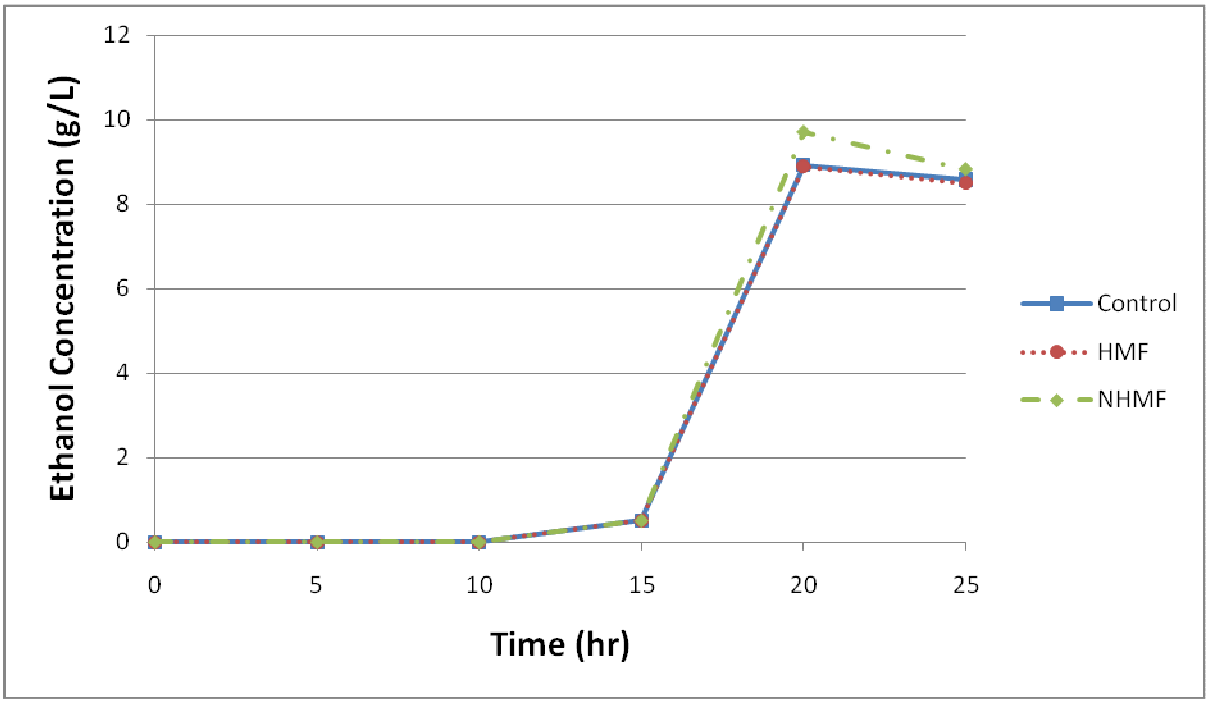

Figure 2.9 Ethanol production for 2% dextrose loading magnetic fermentation.

2.4.3 6% Dextrose Loading Magnetic Fermentation

In this section, the results are given for the 6% dextrose loading rate magnetic experiments. The homogeneous magnetic field was excluded from these experiments because it produced no significant effects during 2% dextrose loading magnetic fermentation experiments. A plot of cell growth data and growth models versus time for the control group and both experimental sets may be seen in Figure 2.10. A plot of ethanol production versus time for all sets may be seen in Figure 2.11. Cell growth was modeled with the previously mentioned logistic growth model; the model parameters for all data sets may be seen in Table 2.4.

Similar to the 2% dextrose loading experiments, the cell growth data shown in Figure 2.10 suggests no difference between the cell growth of the control group and experimental group. Statistical analysis of the model parameters confirmed this observation. Once again, these results are in contrast to those reported in (6) where a non-homogeneous static

magnetic field on the order of hundreds of mT produced a significant difference in cell growth when compared to a control group under no magnetic field.

Figure 2.11 shows ethanol production beginning sometime between hours 12 and 18, after the CFU density surpasses approximately $3x10^5$ CFU/mL. The peak in ethanol production at hour 24 was used to calculate an ethanol yield of 83.0% of the theoretical yield for the NHMF group, and the peak at hour 30 was used to calculate an ethanol yield of 82.9% of the theoretical yield for the control group. This suggests that there is no significant difference between the peak concentrations of the NHMF group and the control group, despite a possible increase in production rate indicated by the NHMF ethanol peak occurring before the control peak. Analysis of the ethanol data using the general linear model procedure confirms no significant difference with a P-value of 0.1671.

The results of the ethanol production analysis of this experiment contrast those of the 2% dextrose loading magnetic fermentations. However, indications of magnetically enhanced fermentations still existed in the 6% dextrose loading experiments. Of the four repetitions, two showed peak ethanol production of the experimental group occurring at a sample time six hours prior to the peak of the control group, suggesting an increased ethanol production rate. However, the final ethanol concentrations of both groups were the same. Despite indications of an increased ethanol production rate, any significance was overshadowed when the four repetitions were averaged for analysis. The inconsistency among these four repetitions may be explained by the numerous factors contributing to ethanol yield; variability within fermentation experiments is a common occurrence.

Despite these inconsistencies, it was determined that further experimentation was not necessary. Even though some statistically significant ethanol production enhancement was observed, the magnitude of enhancement was not large enough to offset the potential cost and difficulties of creating magnetic fields at an industrial scale.

Table 2.4 Cell growth model parameters for 6% dextrose loading magnetic fermentation.

Set	X_0	X_∞	k
Control	720	21×10^7	0.61
Non-homogeneous	720	21×10^7	0.61

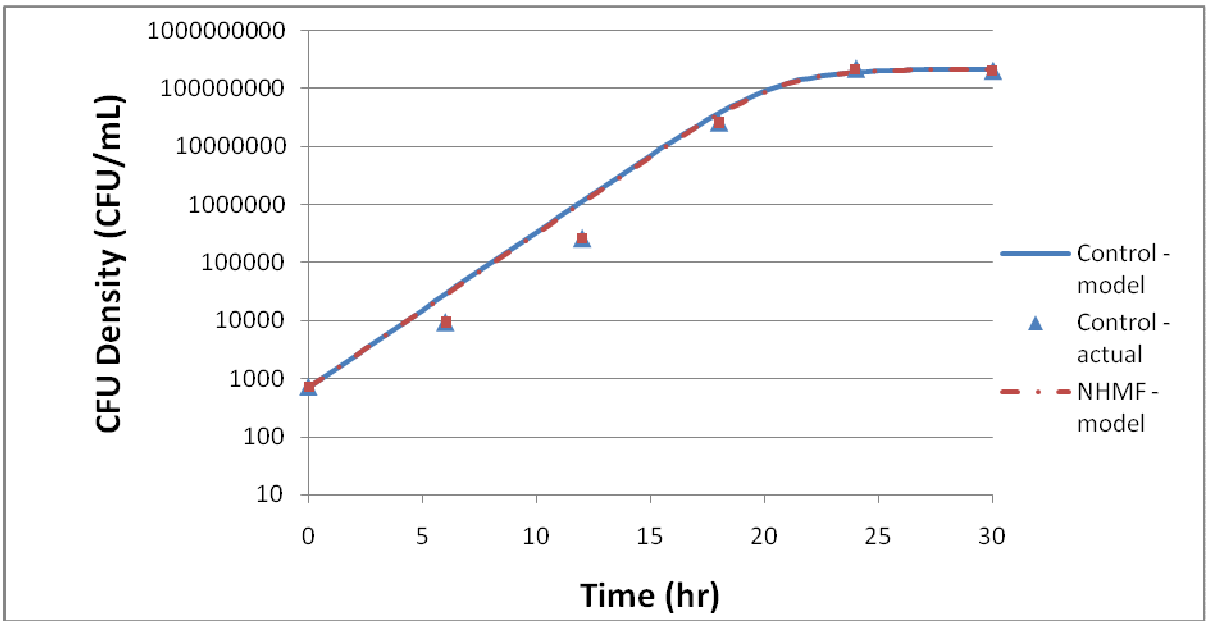

Figure 2.10 Cell growth for 6% dextrose loading magnetic fermentation.

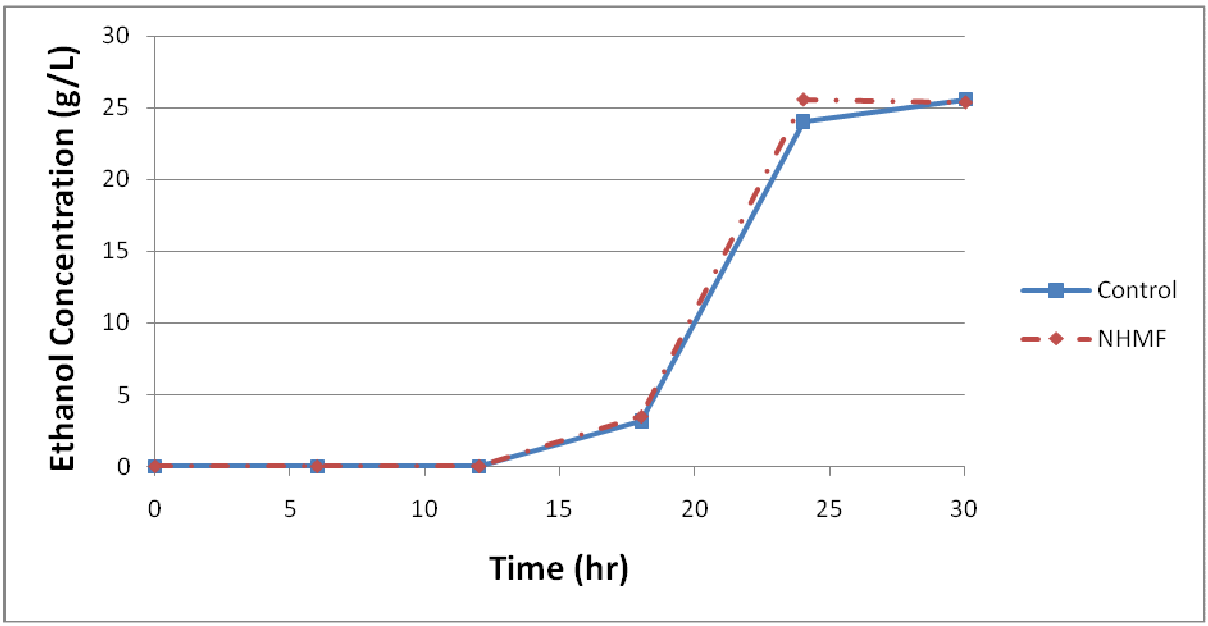

Figure 2.11 Ethanol production for 6% dextrose loading magnetic fermentation.

2.5 Conclusions and Future Work

The objectives of these experiments were to characterize the fermentation kinetics of *S. Cerevisiae* ATCC® 24859 and to determine the effects of magnetic field enhanced fermentation on cell growth and ethanol production with a well-controlled experimental method. The fermentation kinetics of ATCC® 24859 were determined for cell concentration loading rates from 10^2 to 10^7 CFU/mL. These results indicated that starting cell concentrations below 10^6 CFU/mL exhibited consistent logistic cell growth over several hours and a lag in ethanol production which are both desirable traits for magnetic field enhanced fermentation experiments. A starting cell concentration of 10^3 CFU/mL was chosen for all subsequent magnetic fermentation experiments.

Magnetic fermentation experiments with homogeneous and non-homogeneous static magnetic fields showed that the yeast cell growth during fermentation is unaffected by static magnetic fields. This result was consistent across two fermentation medium sugar loading rates.

Conflicting ethanol production results prevent making definite conclusions about the effects of magnetic fields on ethanol production. However, experiment results point to a minimal increase in either peak ethanol production or ethanol production rate during non-homogeneous static magnetic field enhanced fermentations.

Together, these results indicate that magnetic field enhanced fermentation is not practical for industrial application. Creating powerful magnetic fields on small-scale fermentations proved to be cumbersome, even at fermentation volumes much smaller than those used in industrial scale fermentations. The enhancement in ethanol production exhibited in these and other published experiments are also too minimal to offset the cost of permanent magnets or electromagnets capable of producing appreciable magnetic fields at an industrial scale.

It may be advantageous to the scientific and academic communities to complete additional well-controlled experiments in order to further characterize the relationship between ethanol production and magnetic fields. This could include experiments to test the relationship between magnetic field strength and ethanol production enhancement, experiments to test the relationship between alternating magnetic field frequency and ethanol production enhancement, and experiments to better determine the difference in ethanol production enhancement between homogeneous and non-homogeneous static magnetic fields.

CHAPTER 3. MICROFLUIDIC NEMATODE ASSAY

3.1 Introduction

3.1.1 Background

Non-parasitic nematodes, specifically *Caenorhabditis elegans*, have commonly been used in laboratory studies as a model for the study of human aging(16). Their relatively simple cellular composition and nervous system make them prime candidates for such studies. Their transparent bodies and hardiness also readily enable *in vivo* observation. Thus, *C. elegans* is a well studied organism with a large amount of molecular and behavioral information already available.

In contrast, the characterization of parasitic nematodes has been limited by the versatility and resolution of available technology. Current migration assays for parasitic nematodes involve movement through mesh or soil environments and comparing the number of migrated subjects to the number of stationary subjects(17)(18). Though these assays closely model the nematodes' natural soil environment, this method does not enable real time observation of their movements and reactions to various obstacles, which may be used to better define the nematodes' physiological states.

Nematodes achieve forward locomotion through undulatory propulsion. Undulating organisms move forward with uniform speed along a sinuous path of motion(19). This mechanism has intrigued researchers and inspired a number of quantitative models to explain the nature of undulatory motion(19). Distinct parameters of undulatory motion exist, including forward velocity, amplitude, wavelength, period, and frequency. These parameters may be correlated to the physiological state of a nematode.

Parasitic nematodes include several varieties of nematodes that destroy useful resources, resulting in appreciable economic losses. Advancing the technology for studying

parasitic nematodes, leading to better characterization of parasitic nematodes' physiological properties, may help curtail these losses. To better characterize parasitic nematodes and the correlation of their undulatory parameters to their physiological state, it becomes advantageous to develop an assay that enables high resolution, real-time observation of nematode movement. Such an assay would facilitate the comparison of various parasitic nematode species and the effects of anthelmintic drugs, drugs that expel parasitic worms by inhibiting their movement, on nematode undulatory movement. Several experiments have shown that microfluidic platforms are useful for *in vivo* observation of nematodes(20)(21)(22)(23). The previously mentioned reasons necessitate the development of a microfluidic platform that is tailored to the observation of nematode undulatory movement.

3.1.2 Objectives

The objectives of these experiments were to develop a high resolution microfluidic assay for measurement of parasitic nematodes' undulatory locomotive parameters and to complete the characterization and comparison of these parameters for *H. glycines* and two isolates of *O. dentatum*.

3.1.3 Literature Review

3.1.3.1 Microfluidic Platforms and Microfluidic Nematology

Whitesides (2006) reviewed the origins and discussed the future of microfluidics. Early applications of microfluidics mainly involved subject analysis with microfluidic platforms offering advantages such as the ability to use small sample and reagent quantities, the ability to carry out separations and detections with high resolution and sensitivity, low cost, rapid analysis, and small devices. Whitesides suggests that the development of new assays for scientific fields including biomedicine and pharmacology are in the future of

microfluidics. The development of advanced fabrication techniques will also enhance microfluidics.

A review by Sia and Whitesides (2003) describes the use of poly(dimethylsiloxane) for the fabrication of microfluidic systems for biological studies. They state that the properties and fabrication techniques of PDMS microstructures make them suitable for miniaturized biological studies. Their review demonstrates the flexibility of PDMS microfluidic platforms, including uses such as immunoassays, separation of proteins and DNA, sorting and manipulation of cells, studies of cells in microchannels exposed to laminar fluid flow, and large-scale, combinatorial screening. These examples provide a case for the advantages of biological study miniaturization.

Lockery et al. (2008) created several PDMS microfluidic platforms to aid in the study of nematode movement. These platforms include a two-dimensional, artificial soil device and a waveform sampler device. The artificial soil platform consisted of a 1 x 1 cm hexagonal array of cylindrical posts (100 μm dia. by 50 μm height) with a series of input and output ports for the insertion of worms and control of fluid flow. The post array was designed to mimic soil particles or contact points for a nematode crawling in its natural environment. The study found that nematodes in the artificial soil environment exhibited mostly sinuous movement, similar to the crawling observed on an agarose surface. The waveform sampler platform consisted of several microfluidic platforms with sinusoidal channels (50 μm height). A total of six platforms had a constant amplitude (A) of 0.5, 1, or 2 times the natural amplitude of a wild-type *C. elegans* with three wavelengths (λ) per platform of 0.4, 0.6, and 0.8 or 1.0, 2.0, and 3.0 times the natural wavelength of a wild-type *C. elegans*. It was found that nematodes were unable to pass through channels with a small A/λ quotient, as this value is proportional to the amount of tangential thrust exerted during undulatory movement.

Chalasani et al. (2007) created a PDMS microfluidic platform for the study of *C. elegans* olfactory behavior. Their platform enabled the trapping of a single nematode sample, with the head of the nematode protruding into a separate channel. A series of channels were used as a microfluidic chemical delivery system for the flow of isomyl alcohol over the nematode's head while the odor response of AWC neurons was observed with fluorescent imaging. They were also able to observe the turning behavior of the nematode's head evoked from odor removal.

Similarly, Chronis et al. (2007) created PDMS microfluidic platforms for the behavioral and olfactory study of *C. elegans*. The behavioral platform consisted of a tapered channel which restricted a nematode by vertical compression. The behavioral chip was used to correlate a nematode's physical behavior with its neuronal behavior as observed by fluorescent imaging. The olfactory platform functioned in a manner similar to the one described by Chalasani et al. (2007). Commentary on this experiment was provided by Zhang (2007). Zhang specifically mentioned the high degree of control over the dimensions, shape, and physical properties as the prime benefits of using microfluidic "worm chips." Zhang also mentioned adding mechanical or thermal stimuli to future microfluidic platforms to further enhance behavioral study of nematodes.

A PDMS microfluidic platform was also created by Gray et al. (2004). In their research, PDMS platforms were used as an aerotaxis assay to observe the oxygen-related behaviors of *C. elegans.* Within the microfluidic platform, a gas-phase oxygen gradient was created, and the behavior of nematodes was observed as a function of oxygen concentration within an agar substrate.

3.1.3.2 Nematode Migration and Drug Assays

Petersen et al. (1997) observed the migration of adult *O. dentatum* under the influence of the benizimidazole carbamate, oxfendazole, a nematode anthelmintic. Their migration

assay consisted of two plastic tubes, a bottomless 20 mL tube inserted into a 50 mL tube, with a polyamide net of 300, 350, 400, or 500 µm mesh size. Experimental nematodes were exposed to 10 µM oxfendazole doses, and the migration of control and experimental nematodes was monitored for 60 minutes. The migrated nematodes on the other side of the filter were counted, and a percent of inhibition was calculated. The 350 µm mesh size was found to be optimal for the migration assay and was used in subsequent experiments to determine the effects of oxfendazole concentration on the percent inhibition.

Martin et al. (2003) studied the effects of the cholinergic anthelmintic, levamisole, on the migration patterns of two isolates of *O. dentatum*, one levamisole-sensitive (SENS) and another levamisole-resistant (LEVR). The migration assay consisted of two tightly fitting plastic tubes approximately 10 mm in length holding a 20 µm nylon filter. Exsheathed larvae were drugged with levamisole concentrations ranging from approximately 1 µM to 1 mM and added to the top of each migration assay filter. After 2 h incubation at 37˚C, migrated nematodes on the other side of the filter were counted, and a percent of inhibition for each drug concentration was determined. The percent of inhibition is proportional to the drug concentration. The migration of the SENS isolate was inhibited more than the LEVR isolate, even at concentrations as low as 1µM.

3.2 Methods and Procedures

3.2.1 Microfluidic Platform Design and Fabrication

The features of the microfluidic platform were designed to facilitate the observation of nematode undulatory movement. Four parallel microfluidic channels were chosen to enable the simultaneous observation of multiple nematode species, multiples drugs, or multiple drug doses on nematode movement in different channels. Having four channels also ensures constant temperature and light across several nematode sets observed simultaneously. Five designs were created featuring channel widths from 100 to 300 µm in

50 µm intervals. The input ports for each channel were tapered to promote nematode movement from the ports into the channel. A 1 cm ruler was added along the center of the channel to enable real-time calculation of approximate nematode velocity.

The microfluidic platforms used in these experiments were fabricated with standard soft lithography techniques(24). Transparency mask layout was completed in Adobe® Illustrator® CS4 and printed by an outside vendor (Imagesetter Inc., Madison, WI). The mask layout for the 300 µm microfluidic platform may be seen in Figure 3.1.

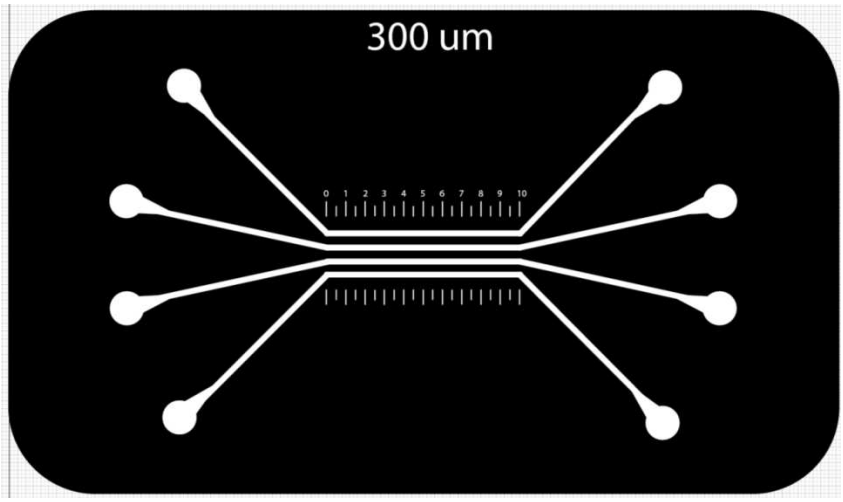

Figure 3.1 Microfluidic platform mask layout featuring 300 µm channels.

Master molds were fabricated on 3" test grade silicon wafer substrates (University Wafer, South Boston, MA) using SU-8 photoresist (Formulation 2-25, MicroChem Corp., Newton, MA)(25). Photoresist adheres best to a clean substrate so silicon wafers may be pretreated with a standard RCA clean and dehydrated by baking for 5 minutes at 200˚C. The silicon wafers purchased for this research were cleaned before packaging so the substrate pretreatment step was skipped to save time and chemical resources. 3 mL of SU-8 (1 mL for each inch of substrate diameter) were added to the center of a wafer via pipette. A spread cycle evenly disperses the photoresist across the substrate by spinning at 500 rpm for 5 s. The spinning rate was then ramped to 1000 rpm for the 25 s spin cycle which resulted in a photoresist layer of approximately 40 µm in thickness. A soft bake for 5 minutes at 65˚C

followed by 15 minutes at 95˚C evaporated the photoresist solvent and increased the layer density. The photoresist coated substrates were then covered with the transparency masks and exposed to 350 to 400 mJ/cm^2 with a near-UV lamp (Omnicure Series 1000, Exfo Photonic Solutions Inc., Mississauga, ON, Canada). Following exposure, a post bake for 1 minute at 65˚C followed by 4 minutes at 95˚C cross-linked the exposed portion of the photoresist layer. The photoresist layer was then developed with SU-8 Developer (MicroChem Corp.) for 6 minutes. Ultrasonication for 1 to 2 s at the beginning of development significantly hastens the development process; however, care must be taken not to overly sonicate the master mold or there is increased risk for the SU-8 features to separate from the substrate. After complete development, the master mold was rinsed with isopropyl alcohol and dried with compressed air. A summary of the master mold fabrication steps may be found in Table 3.1.

Table 3.1 Master mold fabrication steps for 40 µm feature thickness on a 3" silicon wafer.

Step 1	Substrate Pretreatment	RCA clean, bake 5 min @ 200˚C
Step 2	Spin Coat	3 mL SU-8, 5 s @ 500 RPM, 25 s @ 1000 RPM
Step 3	Prebake	5 min @ 65˚C, 15 min @ 95˚C
Step 4	Expose	350-400 mJ/cm^2
Step 5	Post Exposure Bake	1 min @ 65˚C, 4 min @ 95˚C
Step 6	Develop	2 s ultrasonication, 6 min soak w/ hand agitation
Step 7	Rinse and Dry	IPA rinse, dry w/ compressed air

The microfluidic devices were cast over the SU-8 master molds in PDMS (Sylgard 184 Silicone Elasomer, Dow Corning Corp., Midland, MI) mixed from base and curing agent at a 10:1 ratio by weight, respectively. During mixing of the base and curing agent, excessive air bubbles formed in the PDMS so they were removed by placing the PDMS in a vacuum chamber. A master mold was placed in a 100x15 mm Petri dish and 22 g of PDMS

were added. The PDMS was cured by heating the Petri dish on a hot plate at 70˚C for 2 h. After curing, the PDMS was cut with a utility knife and slowly peeled from the master mold. Ports were punched in the PDMS with a hollow 8 gauge needle. Finally, the PDMS was bonded to an individual glass coverslip by exposing both to air plasma for 35 s before joining the two and applying light pressure. A completed microfluidic platform may be seen in Figure 3.2. A summary of the microfluidic device fabrication steps may be found in Table 3.2.

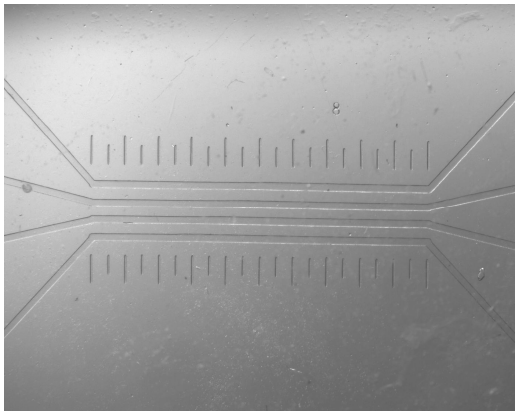

Figure 3.2 Microfluidic channels developed for observation of nematode undulatory parameters.

Table 3.2 Microfluidic device fabrication steps.

Step 1	Mix	22 g PDMS, 10:1 mix ratio by weight
Step 2	Bubble Removal	Vacuum chamber until transparent
Step 3	Pour and Cure	2 h @ 70˚C
Step 4	Peel	
Step 5	Ports	Punch w/ 8 gauge hollow needle
Step 6	Bond	35 s air plasma exposure

3.2.2 Nematode Preparation

Two parasitic nematode species were observed for this research: *Oesophagostomum dentatum*, a nodular intestinal nematode parasite of pigs, and *Heterodera glycines*, a soybean cyst nematode(26). *H. glycines*, or soybean cyst nematode (SCN), specimens were obtained from the lab of Dr. Thomas Baum of Iowa State University's Department of Plant Pathology. *O. dentatum* specimens were obtained from the lab of Dr. Richard Martin of Iowa State University's Department of Biomedical Sciences in the College of Veterinary Medicine. Furthermore, two isolates of the *O. dentatum* species were tested: levamisole-sensitive (SENS) larvae which are sensitive to the cholinergic anthelmintic, levamisole, and levamisole-resistant (LEVR) larvae which have developed a resistance to the drug.

Prior to experiments, a 1% (w/v) agarose solution was mixed and heated to 100˚C. The liquid agar solution was cooled to 37°C in a warm water bath and a small volume (~0.5 mL) of concentrated nematode solution was added by pipette. The nematodes were thoroughly mixed into the agar and allowed to stabilize at 37°C for 20 minutes. The agar-nematode solution was injected into the 300 µm width microfluidic channels via 1 mL syringe and rubber tubing.

O. dentatum larvae are encased in a protein sheath while in a soil-dwelling larval state. After ingestion, the acidic stomach environment causes the nematode to shed its sheath as it is ready to enter the adult phase of its life cycle. In these experiments, both sheathed and exsheathed *O. dentatum* specimens were observed. Shedding of the protein sheath was incited by mixing nematode solution with 10% bleach solution at a 5:1 volume to volume ratio, respectively. A small sample of the nematode solution was observed under microscope until the majority of the nematodes had shed their sheath as shown in Figure 3.3. The nematode-bleach solution was then diluted with tap water, centrifuged at 5000 rpm for 1 minute, and excess liquid is aspirated with a pipette. This rinsing process was completed

three times to cleanse the nematodes of residual bleach. Preparation of the exsheathed *O. dentatum* specimens was then completed as described above.

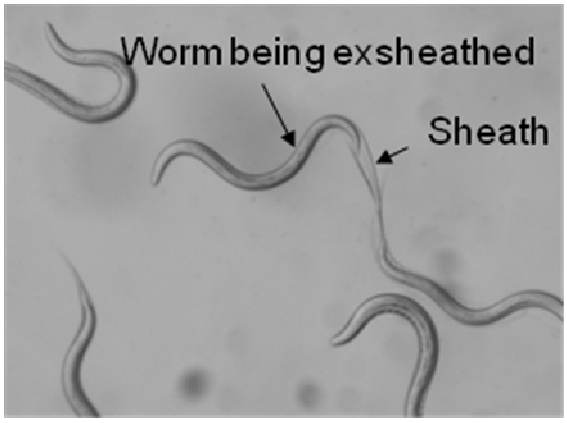

Figure 3.3 Exsheathing of *O. dentatum* with bleach solution.

3.2.3 Data Capture and Analysis

Subjects were observed with a Leica MZ16 transmission stereomicroscope (Leica Microsystems Inc., Bannockburn, IL) featuring dual 1X and 2X objective lenses that enable magnification from 7.1X – 230X. A QImaging QICAM 12-bit Mono Fast 1394 Cooled digital camera (QImaging, Surrey, BC, Canada) interfaces with QImaging QCapture PRO software enabling capture of individual digital images and digital image sequences.

Digital image sequences of nematode movement were captured at one second intervals and a resolution of 1392x1040 pixels using QCapture PRO software and saved in uncompressed .avi video format. These videos may be analyzed with QCapture PRO or imported into MATLAB for analysis of individual frames. An actual distance to pixel distance ratio was created by measuring the pixel width of a channel of known width using the MATLAB Image Toolbox as shown in Figure 3.4. This ratio was used to translate pixel measurements to actual distance for the calculation of nematode velocity, amplitude, and wavelength.

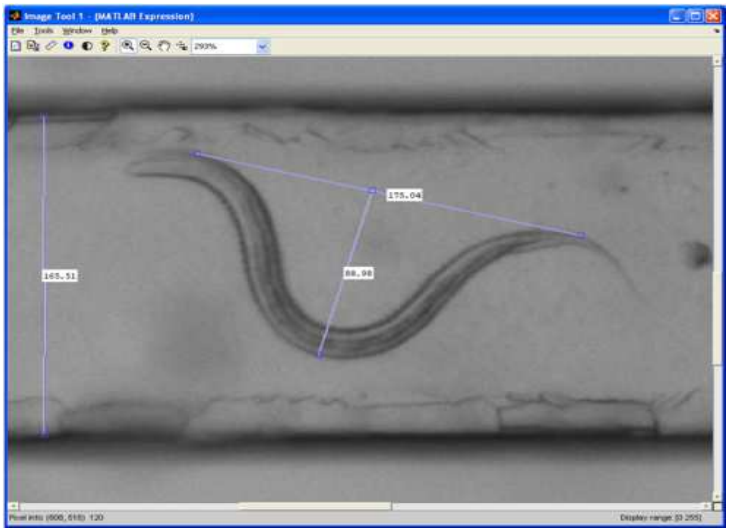

Figure 3.4 Measurement of channel pixel distance and nematode amplitude and wavelength in the MATLAB Image Toolbox.

Nematodes with unimpeded forward propagation exhibit a consistent velocity over distances much longer than their body length(19). For this experiment, nematode velocity (v) was defined as the linear distance traveled along a channel by the head over a period of time as shown in Figure 3.6a. This velocity was recorded for nematodes traveling a distance on the order of several times their intrinsic body length through a straight microfluidic channel with uninterrupted forward movement. Average velocity over the traversed distance is measured by obtaining the total number of pixels traveled by the head of a nematode in a 1 Hz digital image sequence. The total number of pixels traveled between beginning and end frames is calculated using QCapture PRO software and translated to an actual distance using the previously mentioned pixel-distance ratio. Actual distance was divided by the total number of frames between the initial and final measurement positions to obtain a velocity in the units of micrometers per second. Figure 3.5 demonstrates the velocity measurement process.

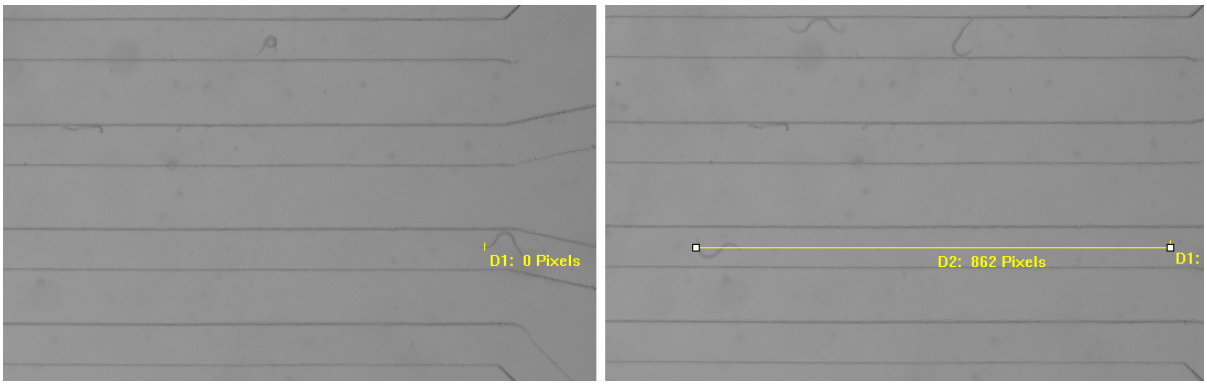

Figure 3.5 Nematode velocity measurement at the initial and final positions.

Nematode bodies form a natural sinuous shape during forward locomotion(19): amplitude (A) is measured from latitudinal peak to peak while wavelength (λ) is measured from longitudinal peak to peak as shown in Figures 3.6b and 3.6c, respectively. Videos of nematode movement for determining amplitude and wavelength were recorded at a higher magnification than those recorded for determining velocity in order to maximize the resolution of a single specimen and to enable accurate measurements. The pixel distances of these attributes were measured using the MATLAB Image Toolbox as shown in Figure 3.4. Pixel distance was converted to actual distance in the units of micrometers using the previously mentioned pixel-distance ratio. Amplitude and wavelength measurements were only completed on worms that were normal to the viewing plane and clearly exhibited forward movement that was uninhibited by channel walls or other obstacles (air bubbles, other worms, etc.). This prevented distortion of their natural amplitudes and wavelengths.

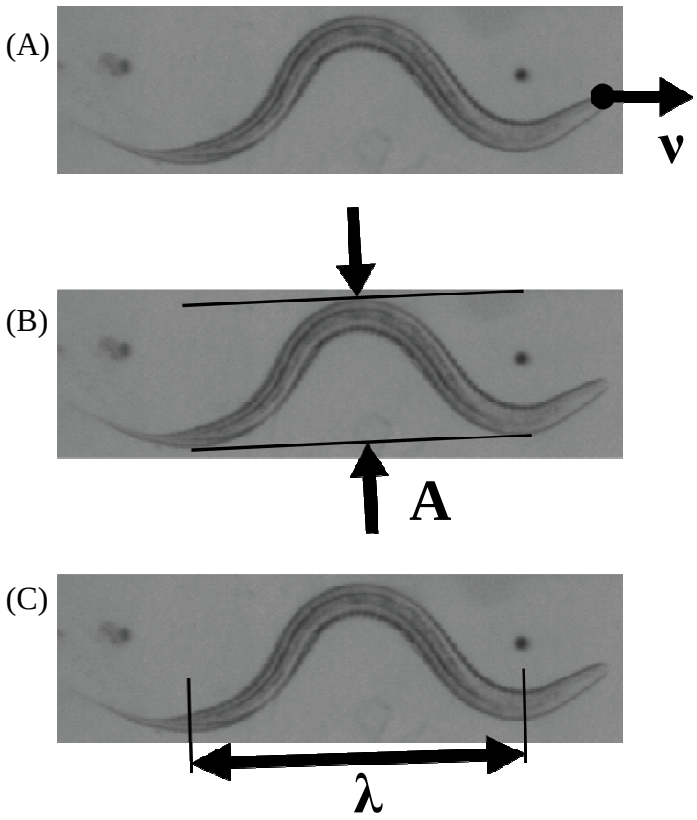

Figure 3.6 Undulatory motion parameters: (A) velocity, (B) amplitude, (C) wavelength.

The traveling wave relationship describes the relationship between the velocity, frequency, and wavelength of a sinusoidal wave. Nematodes moving sinusoidally with uniform velocity and wavelength should have a specific frequency of undulatory movement. The frequency of nematode movement was defined as the inverse of the time period taken to return to an initial state of motion. This is demonstrated in Figure 3.7 where the shape of the nematode's body is approximately the same in the first and last frames. Measurement of nematode frequency was completed by analyzing a sequence of 1 Hz video frames for nematodes exhibiting uninterrupted forward velocity. The shape of the nematode body was observed and the number of frames between similar initial and final shapes was defined as the period. The inverse of the period yielded the frequency.

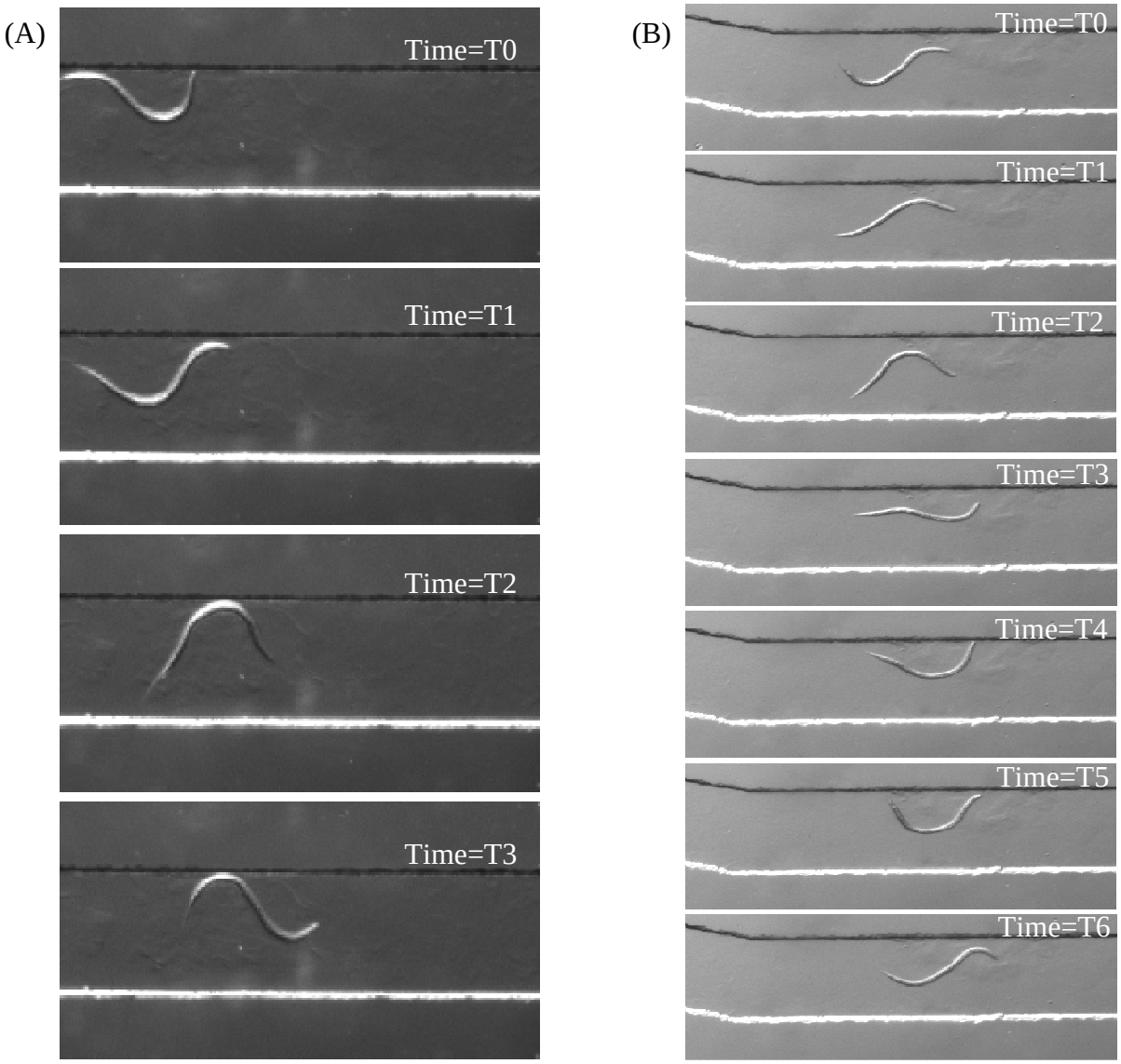

Figure 3.7 Frequency calculation of (A) *O. dentatum* and (B) *H. glycines*.

3.2.3 Statistical Analysis

Nematode movement observation trials were conducted using a randomized complete block design with at least three replications for each undulatory parameter studied. Statistical analysis of all data was completed with GraphPad Prism V5.01 (GraphPad Software Inc., San Diego, CA). Comparison of multiple means was performed with a two-way analysis of

variance (ANOVA). Comparison of two means was performed with a t-test. All comparisons were determined to be significant at $p < 0.05$.

3.3 Results and Discussion

3.3.1 Velocity

Analysis of the videos recorded for velocity revealed a subtle but significant difference between the velocities of the two *O. dentatum* isolates. The mean velocities for three days of experiments may be seen in Figure 3.8. This data shows considerable variation from day to day, but there is a continuing trend of the LEVR specimens having greater velocity. A two-way ANOVA of this data revealed the isolate source as 7.65% of the total variation, yielding a P-value of 0.0002. Over three days of experiments, the mean of mean velocities of the sheathed SENS isolate was 122.9 µm/s with a standard deviation of 15.5 µm/s while the sheathed LEVR isolate was 143.7 µm/s with a standard deviation of 16.0 µm/s. A paired t-test revealed no significant difference between the two mean velocities, likely caused by the day to day variation.

Further experimentation showed that the velocity of exsheathed SENS specimens showed a decrease of approximately 12% compared to the sheathed SENS specimens while the exsheathed LEVR specimens showed a decrease of approximately 25% compared to the sheathed LEVR specimens. Exposing the SENS isolate to a dose of 1 µM levamisole caused velocity decrease of approximately 32% while LEVR isolate exposure only resulted in a 25% decrease. The velocity of *H. glycines* showed a slight amount of day-to-day variation in mean but a consistent standard deviation. Over three days of experiments, the mean of mean velocities of the SCN was 42.81 µm/s with a standard deviation of 10.75 µm/s. An unpaired t-test between the amplitude of the sheathed SENS isolate and the SCN yielded a P-value less than 0.0001, confirming a statistically significant difference between the two species'

velocities. A comparison of mean amplitudes among the various *O. dentatum* groups and *H. glycines* may be seen in Figure 3.9.

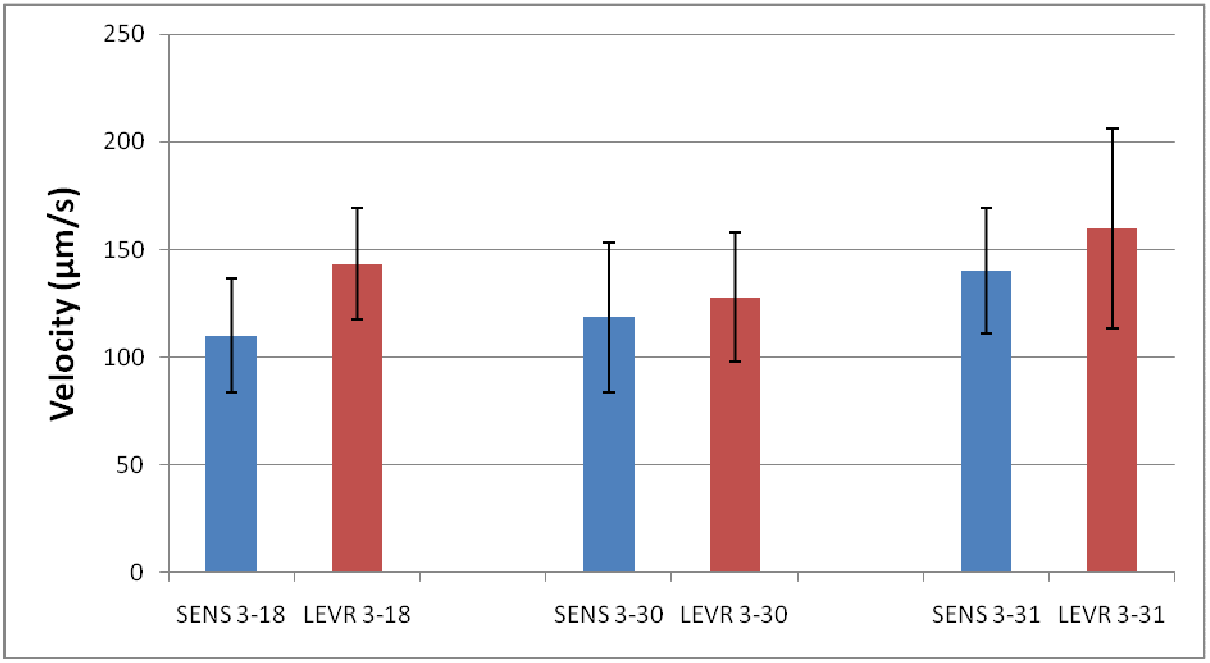

Figure 3.8 Velocity analysis of sheathed *O. dentatum* isolates over three days of experimentation.

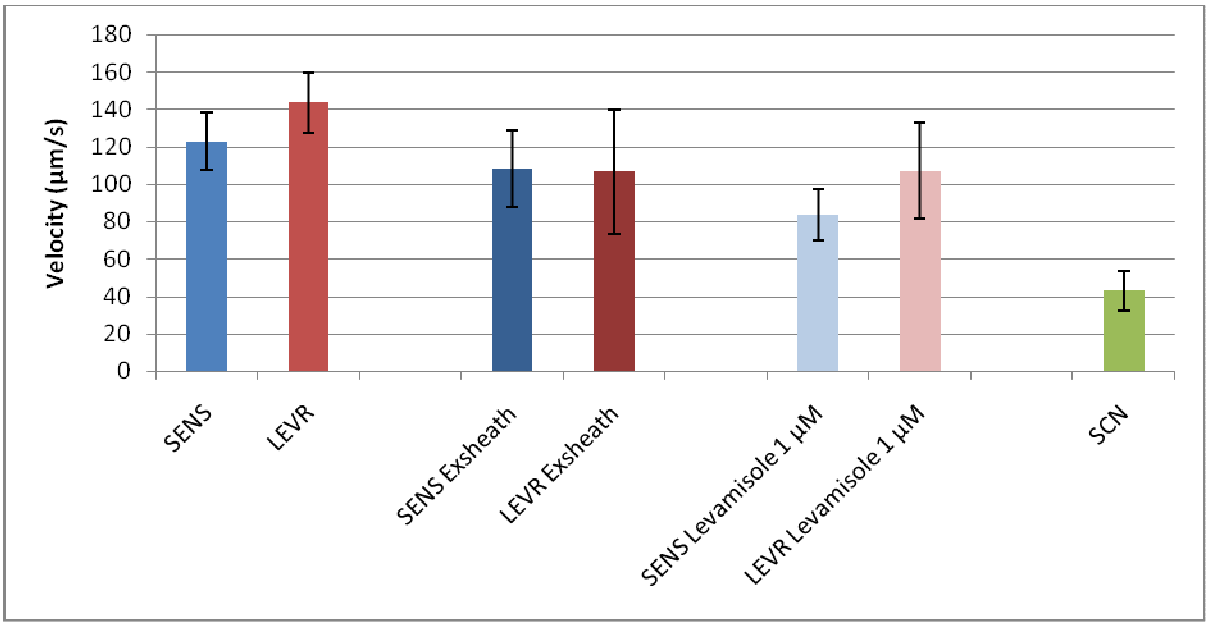

Figure 3.9 Comparison of the average velocity of *H. glycines* and sheathed, exsheathed, and drugged *O. dentatum*.

Velocity data for the exsheathed and drugged *O. dentatum* specimens proved to be difficult to collect and resulted in large day-to-day variation in the mean velocity. The exsheathing process caused some nematodes to curl into a state of paralysis, limiting the number of nematodes to observe. Drugging the nematodes with levamisole caused many of the SENS isolates to move erratically, making their velocity difficult to determine and lowering the number of available sampling points. The LEVR isolate showed a considerable drop in velocity under exsheathing and drugging; however, the standard deviation for both was also large suggesting that the data may be skewed for the previously mentioned reasons. Continued experimentation with exsheathing and drugging is recommended to improve the method for each which should result in increased data consistency.

3.3.2 Amplitude

Analysis of the videos recorded for amplitude and wavelength revealed a significant difference between the sinuous shapes of the two *O. dentatum* isolates. As shown in Figure 3.10, the amplitude of the sheathed SENS isolate tends to be larger than the LEVR isolate. The mean amplitudes for five days of experiments may be seen in Figure 3.11. From this data, it is clear that day-to-day variation in amplitude is relatively low with consistent standard deviation from the mean, suggesting a statistically relevant trend. A two-way ANOVA of this data revealed the isolate source as 7.97% of the total variation, yielding a P-value less than 0.0001. Over five days of experiments, the mean of mean amplitudes of the sheathed SENS isolate was 143.4 µm with a standard deviation of 2.372 µm while the amplitude of the sheathed LEVR isolate was 125.7 µm with a standard deviation of 5.345 µm. A paired t-test yielded a P-value of 0.0002, confirming a statistically significant difference between the amplitude of the two isolates.

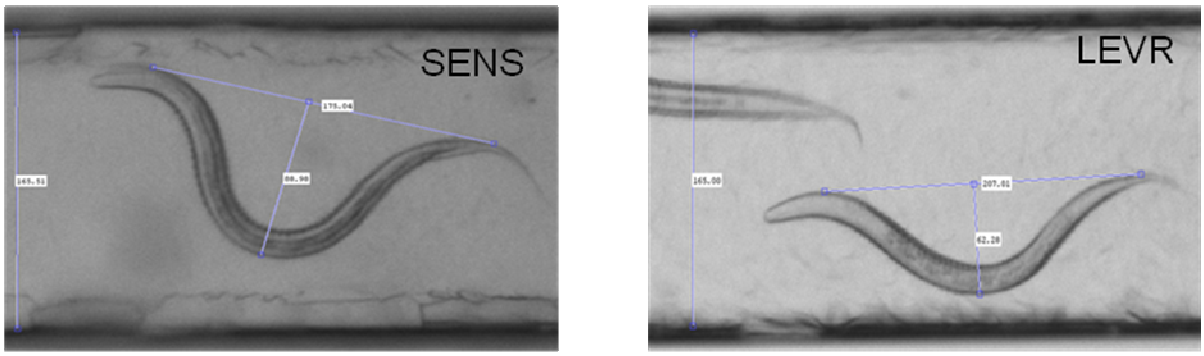

Figure 3.10 The *O. dentatum* SENS isolate exhibits a significantly larger amplitude than the LEVR isolate.

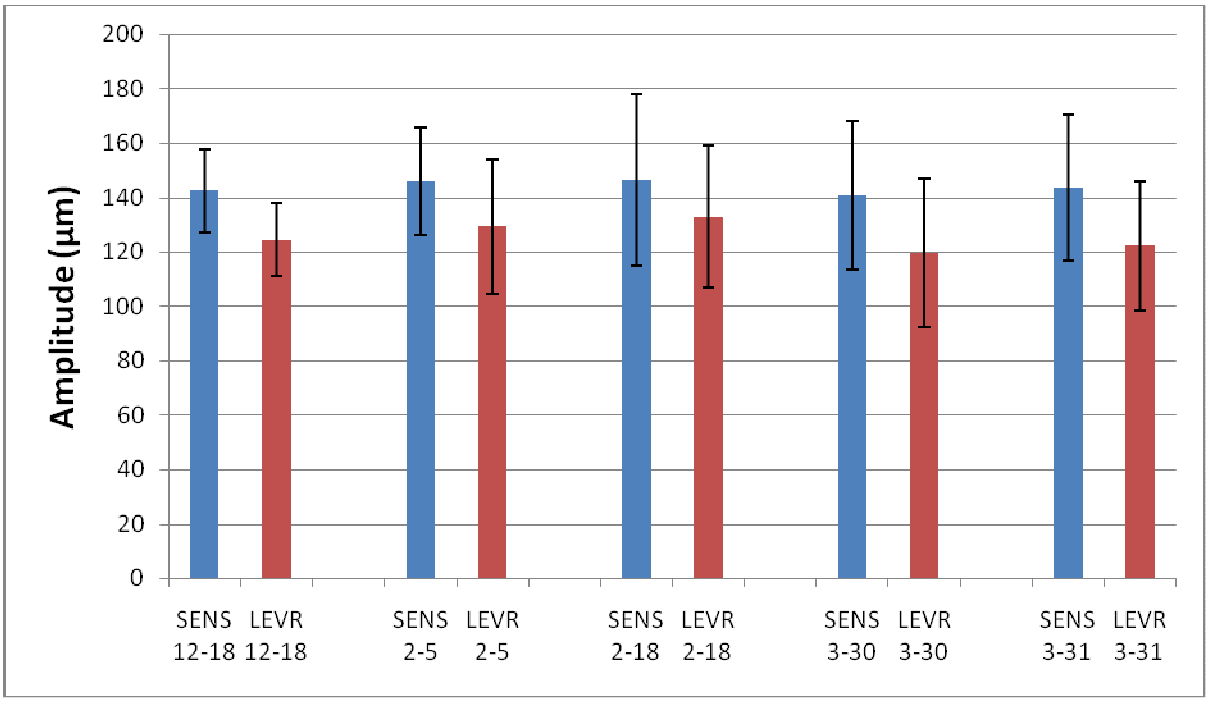

Figure 3.11 Amplitude analysis of sheathed *O. dentatum* isolates over five days of experimentation.

Further experimentation showed that exsheathed *O. dentatum* specimens from both isolates showed a decrease in amplitude of approximately 11% compared to the sheathed *O. dentatum* specimens. Exposing both *O. dentatum* isolates to a dose of 1 µM levamisole caused a 29.4% decrease in amplitude for SENS and only an 8.0% decrease in amplitude for LEVR compared to sheathed *O. dentatum* specimens. Like *O. dentatum*, the amplitude of *H.*

glycines showed consistent daily means and standard deviation. Over three days of experiments, the mean of mean amplitudes of the SCN was 89.63 µm with a standard deviation of 4.961 µm. An unpaired t-test between the amplitude of the sheathed SENS isolate and the SCN yielded a P-value less than 0.0001, confirming a statistically significant difference. A comparison of mean amplitudes among the various *O. dentatum* groups and *H. glycines* may be seen in Figure 3.12.

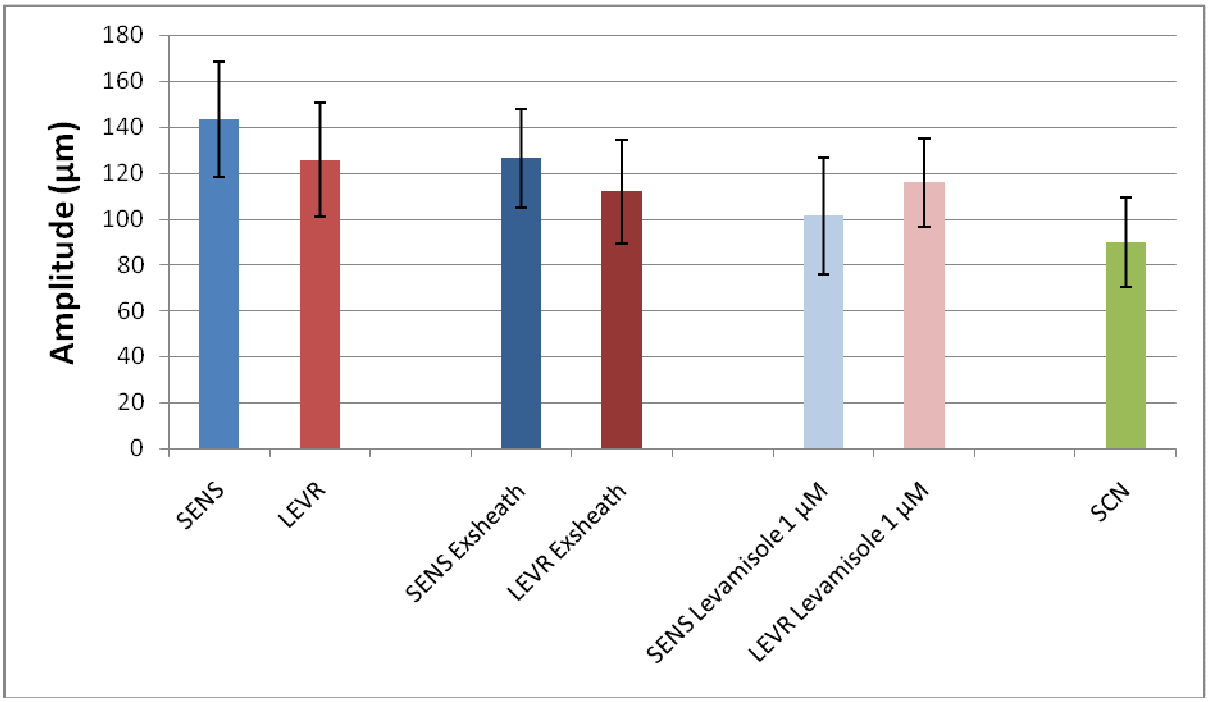

Figure 3.12 Comparison of the average amplitude of *H. glycines* and sheathed, exsheathed, and drugged *O. dentatum*.

The data for *O. dentatum* shows that the amplitude varies significantly with exsheathing and drugging. The most pronounced change can be seen in the amplitude of the drugged SENS nematodes. The mean amplitude for *H. glycines* is consistent with the smaller size of the plant parasite nematode.

These results offer a logical explanation to the difference in velocity seen between the two sheathed *O. dentatum* isolates. The amplitude of the SENS isolate was higher on

average, meaning the head of the SENS nematode has larger side to side movement as it travels sinusoidally. Because the velocity of the nematode is measured as the linear distance traveled down the channel, it does not account for differences in this side to side motion and results in a larger average velocity for the LEVR isolate.

3.3.3 Wavelength

Analysis of the videos recorded for amplitude and wavelength revealed a subtle but significant difference between the wavelengths of the two *O. dentatum* isolates. The mean wavelengths for five days of experiments may be seen in Figure 3.13. This data shows consistent difference between the two isolates despite some day-to-day variation in mean wavelength, suggesting a statistically relevant trend. A two-way ANOVA of this data revealed the isolate source as 2.78% of the total variation, yielding a P-value of 0.0002. Over five days of experiments, the mean of mean wavelengths of the sheathed SENS isolate was 350.3 µm with a standard deviation of 28.15 µm while the wavelength of the sheathed LEVR isolate was 365.3 µm with a standard deviation of 21.44 µm. A paired t-test yielded a P-value of 0.0108, confirming a statistically significant difference between the wavelengths of the two isolates.

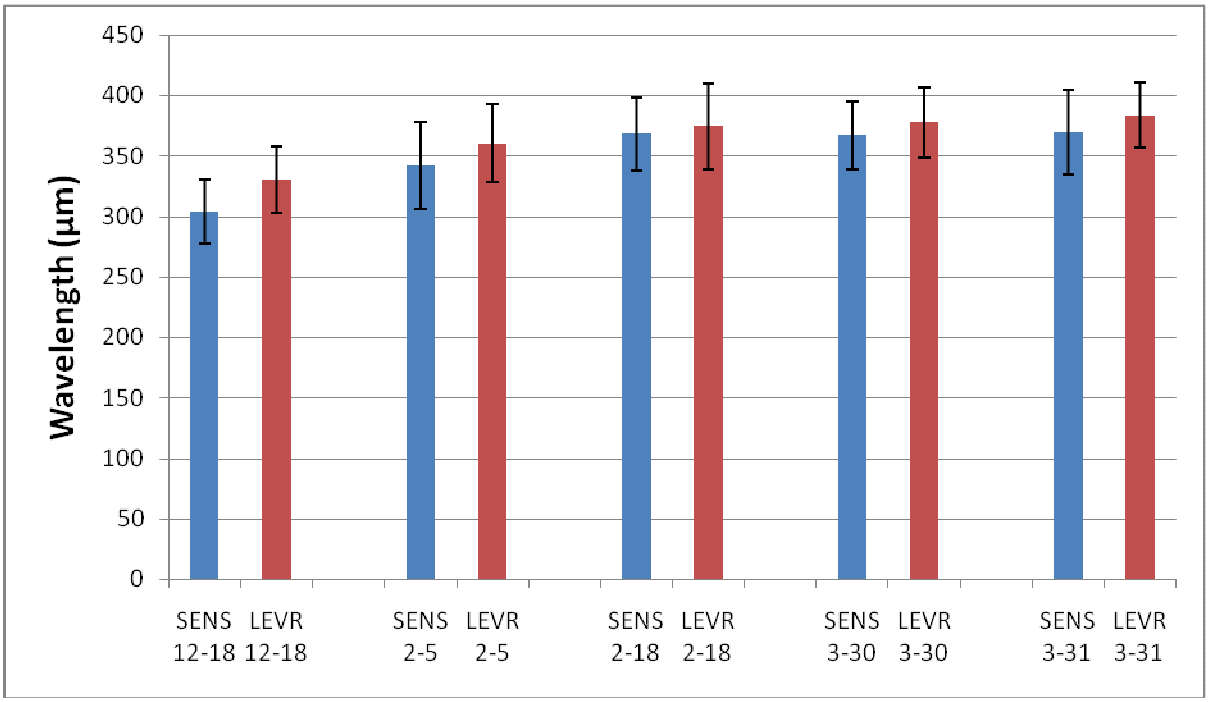

Figure 3.13 Wavelength analysis of sheathed *O. dentatum* isolates over five days of experimentation.

Further experimentation indicated that exsheathed *O. dentatum* specimens from both isolates showed a decrease in wavelength of approximately 7% compared to the sheathed *O. dentatum* specimens. Exposing both *O. dentatum* isolates to a dose of 1 µM levamisole caused a negligible change in wavelength compared to sheathed *O. dentatum* specimens. The wavelength of *H. glycines* showed consistent daily means and standard deviation. Over three days of experiments, the mean of mean wavelengths of the SCN was 310.2 µm with a standard deviation of 21.47 µm. An unpaired t-test between the wavelength of the sheathed SENS isolate and the SCN yielded a P-value of 0.0802, indicating that the difference was not significantly different. A comparison of mean wavelengths among the various *O. dentatum* groups and *H. glycines* may be seen in Figure 3.14.

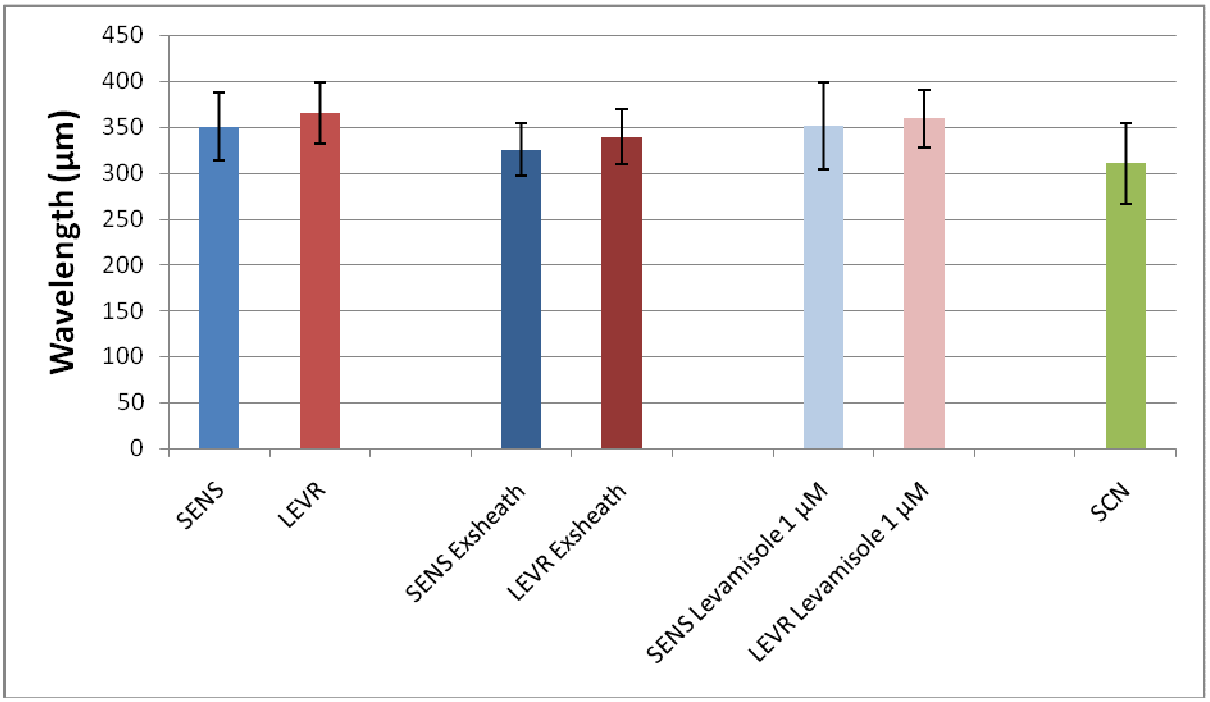

Figure 3.14 Comparison of the average wavelength of *H. glycines* and sheathed, exsheathed, and drugged *O. dentatum*.

The data for *O. dentatum* shows that the wavelength varies little with drugging, in contrast to the amplitude. Though there appears to be a significant change caused by exsheathing, the data set for exsheathed *O. dentatum* was smaller than the sheathed data set, which suggests continued testing could lessen or eliminate the difference. The mean wavelength for *H. glycines* is consistent with the smaller size of the plant parasite nematode. Even though no statistical significance was found with an unpaired t-test of the sheathed SENS and SCN wavelengths, it is likely that continued data collection and a paired t-test would reveal a statistically significant difference.

3.3.4 Frequency

Velocity data and wavelength data were collected independently from one another from different videos. Frequency analysis was completed as a cross reference for the velocity and wavelength data to ensure that together they produced a valid frequency. An

expected frequency for all nematode sets was found by dividing the mean velocity by the mean wavelength. The calculated frequency was found by observing video frames and taking the inverse of the nematodes' periods. Comparison of the calculated and expected frequencies for all nematode sets may be seen in Figure 3.15.

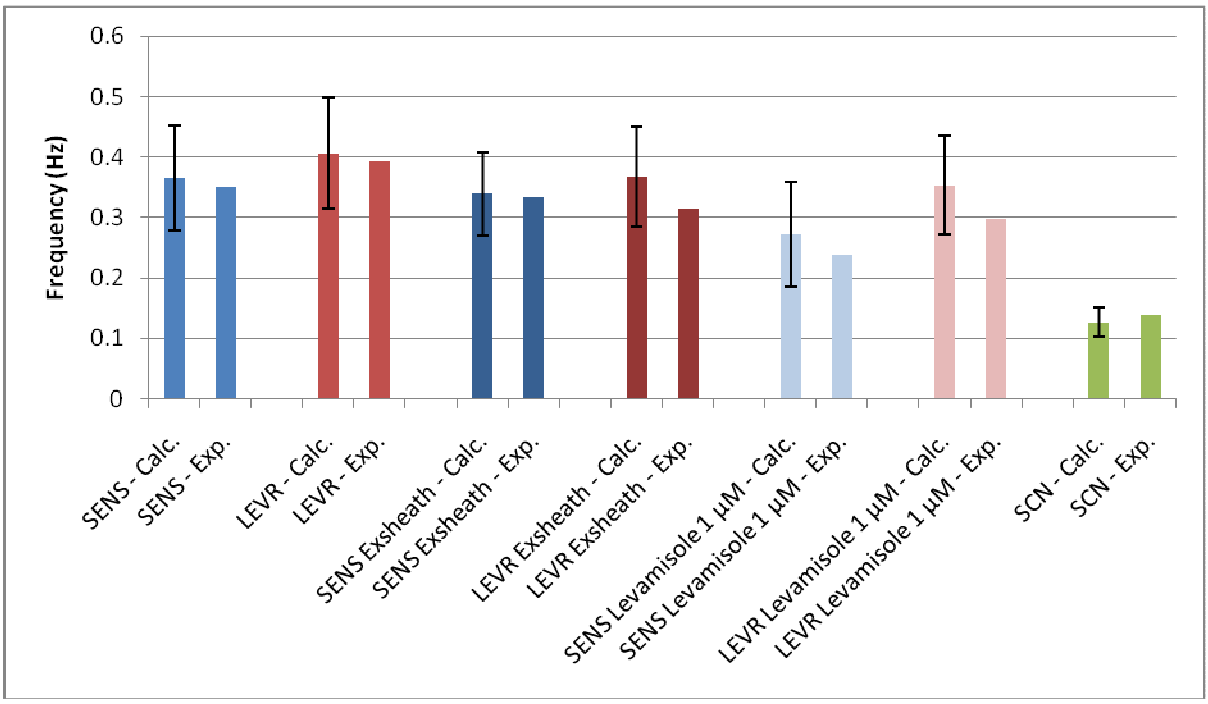

Figure 3.15 Calculated and expected frequencies of *H. glycines* and sheathed, exsheathed, and drugged *O. dentatum*.

No formal statistical analysis of frequency data is included in this thesis because the accuracy of the data is limited by the low temporal resolution used during video capture (1 Hz). Regardless, it is clear that all calculated frequencies were reasonably close to the expected frequencies, confirming the validity of the velocity and wavelength calculations. More accurate frequency calculation could be obtained from videos with higher temporal resolution, but this resolution is limited by the speed of the camera used and the hard disk storage necessary for storing uncompressed videos.

3.3.5 Amplitude/Wavelength Quotient

Perhaps the most interesting aspect of nematode undulatory movement involves both the amplitude and wavelength. Lockery et al. (2008) followed Gray's (1953) theoretical analysis of undulatory motion to determine that the maximum tangential thrust, F_T, exerted by a half-wave is proportional to the quotient of the amplitude and wavelength, A/λ, as shown by the following relationship:

$$F_T \propto \frac{2\pi A/\lambda}{\sqrt{1+(2\pi A/\lambda)^2}}$$

As shown in Figure 3.16, the body of a nematode may be segmented, with each individual segment applying tangential force, resulting in forward propulsive motion. The proportionality of the tangential force and the A/λ quotient shows that a nematode with a larger amplitude, or shorter wavelength, than another should be able to move forward with stronger force.

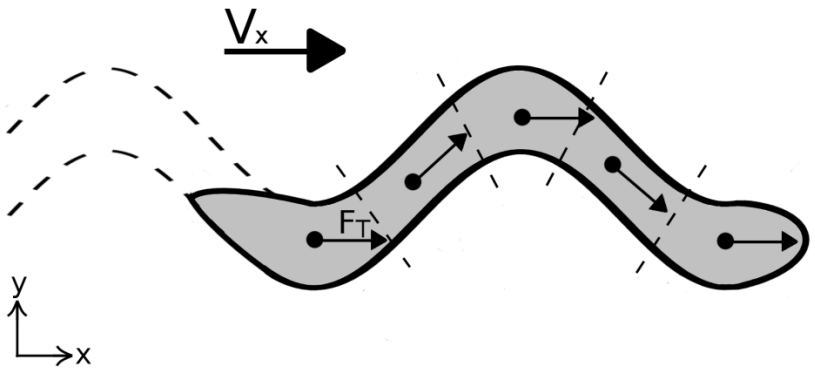

Figure 3.16 Tangential force exerted by each segment of the nematode body causes forward locomotion.

The data gathered for the amplitude and wavelength analysis was combined to produce a set of A/λ quotients. The mean A/λ quotients for five days of sheathed *O. dentatum* experiments may be seen in Figure 3.17. This data shows relatively low day–to-day variation in A/λ with consistent standard deviation from the mean, suggesting a statistically relevant trend. A two-way ANOVA of this data revealed the isolate source as 12.71% of the total

variation, yielding a P-value less than 0.0001. Over five days of experiments, the mean of mean A/λ quotients of the sheathed SENS isolate was 0.4151 with a standard deviation of 0.035, while the sheathed LEVR isolate was 0.346 with a standard deviation of 0.027. A paired t-test yielded a P-value of 0.0008, confirming a statistically significant difference between the A/λ quotients of the two isolates.

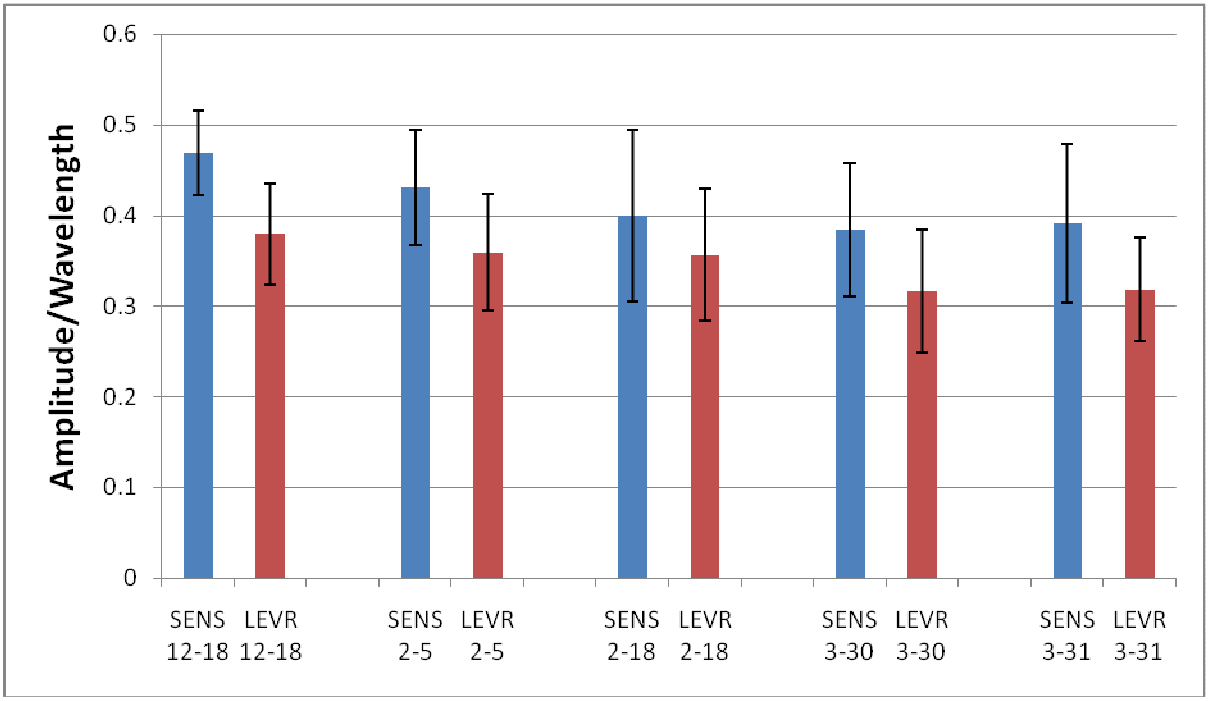

Figure 3.17 A/λ analysis of sheathed *O. dentatum* isolates over five days of experimentation.

The mean A/λ quotients of exsheathed SENS specimens showed a decrease of approximately 6% compared to the sheathed SENS specimens while the exsheathed LEVR specimens showed a decrease of approximately 5% compared to the sheathed LEVR specimens. Exposing the SENS isolate to a dose of 1 µM levamisole caused an A/λ decrease of approximately 31% while LEVR isolate exposure only resulted in a 7% decrease. Over three days of experiments, the mean of mean A/λ quotients of the SCN was 0.2946 with a standard deviation of 0.0047. An unpaired t-test between the A/λ quotients of the sheathed SENS isolate and the SCN yielded a P-value of 0.0010, indicating a significant difference. A

comparison of mean *A/λ* quotients among the various *O. dentatum* groups and *H. glycines* may be seen in Figure 3.18.

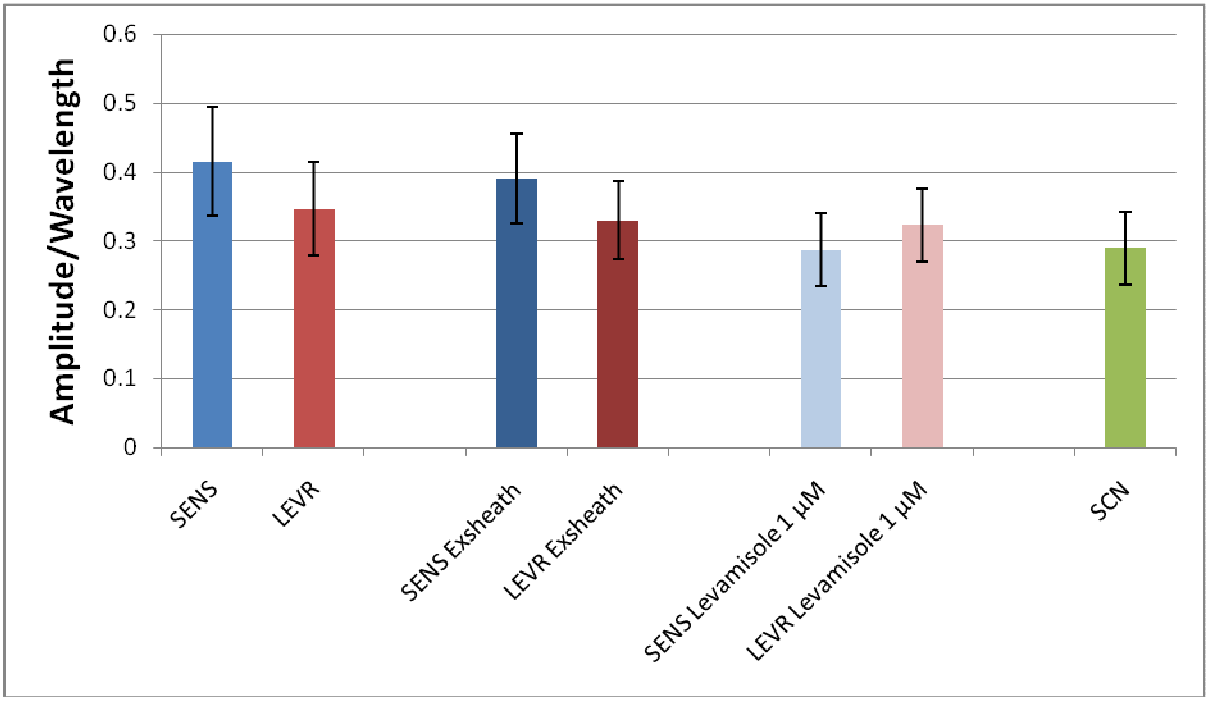

Figure 3.18 Comparison of the average A/λ of *H. glycines* and sheathed, exsheathed, and drugged *O. dentatum*.

The results of the *A/λ* quotient comparisons between the two isolates and between the two species create interesting implications. A significantly lower *A/λ* quotient for the LEVR isolate indicates less locomotive force, and suggests that long-term exposure to levamisole has increased the isolate's resistance to the drug but has also lowered its vigor. After drug exposure, the *A/λ* quotient of the SENS isolate is drastically decreased to a value less than that of the LEVR isolate. This indicates that the SENS isolate has less propulsive force which is supported by the results of Martin et al. (2003) where SENS migration was inhibited more than LEVR migration after a levamisole dose of 1 µM concentration. The animal parasitic nematode, *O. dentatum*, showed a significantly larger *A/λ* quotient than the plant parasitic nematode, *H. glycines*, suggesting that *O. dentatum* has greater propulsive force.

This result is logical because *O. dentatum* must be able to move in both soil and animal digestive tract environments during its life cycle.

3.4 Conclusions and Future Work

The objectives of these experiments were to develop a high resolution microfluidic assay for measurement of parasitic nematodes' undulatory locomotive parameters and to complete characterization and comparison of these parameters for *H. glycines* and two isolates of *O. dentatum*. A microfluidic platform that consisted of straight, parallel channels and ports for adding contents via syringe or pipette was designed. Several platforms of varying channel widths were created. These platforms were fabricated using standard soft lithography techniques.

Microfluidic platforms of 300 μm channel width and a stereomicroscope stage were used to record digital videos of the undulatory movement of *H. glycines* and sheathed, exsheathed, and levamisole drugged *O. dentatum*. These videos were analyzed to determine the velocity, amplitude, wavelength, and frequency of the nematodes.

After the analysis of the recorded nematode undulatory parameters, it is apparent that a difference exists between the physiological states of the *O. dentatum* isolates. A significantly lower A/λ quotient for the LEVR isolate indicates less locomotive force, and suggests that long term exposure to levamisole has increased the isolate's resistance to the drug but has also lowered its vigor. It is also apparent that a difference exists between the two species studied. The animal parasitic nematode, *O. dentatum*, showed a significantly larger A/λ quotient and velocity than the plant parasitic nematode, *H. glycines*, suggesting that *O. dentatum* is the more physically fit of the two. This result is logical because *O. dentatum* must be able to survive in the harsher environment of the pig's digestive tract.

The results of this research suggest that the presented microfluidic platform is a viable migration and chemotaxis assay for the rapid, high-resolution characterization of

nematode drug reactions. This assay offers an advantage over currently used soil or mesh based assays because it enables real-time observation of nematodes' movements and their acute physical reactions to obstacles or chemicals.

In the future, it would be advantageous to continue using this microfluidic platform as a migration and chemotaxis assay to characterize the effects of various drugs on various nematodes. The device was designed for maximum efficiency when testing multiple drugs, drug concentrations, or nematodes. These traits should be confirmed through further use of the assay. Additional research should be completed to find a non-destructive repellent to encourage the movement of nematodes from the ports into the channels. This would greatly increase the ease of the assay's use. The design of ports that are better designed to interface with commonly available specimen transfer tools is also imperative. Finally, the research of Lockery et al. (2008) should be extended to find a three-dimensional soil analog within a microfluidic channel. This would create a more realistic environment for nematode migration and drug chemotaxis assays.

CHAPTER 4. GENERAL CONCLUSIONS

Bioengineering was placed on the Electrical and Computer Engineering department's list of strategic research areas. The objective of this research was to facilitate the growth of a bioengineering center of excellence within the ECpE department by completing cutting edge bioengineering research that required skills and resources from both the life sciences and engineering.

The effects of static magnetic fields on the growth of yeast cells and the production of ethanol during fermentation were observed. This research will benefit the areas of energy, biorenewable resources, and biological systems. During this multidisciplinary effort, the skills of individuals from ECpE, Agricultural and Biosystems Engineering, and Agronomy were utilized to perform effective research in a field that has implications on the future of Iowa's economy and the ecological status of the planet.

A microfluidic platform was designed, fabricated, and used to study nematode undulatory movement. This research will benefit parasitology, nematology, and biomicro systems. Individuals from ECpE and the College of Veterinary Medicine collaborated in this multidisciplinary effort to produce a unique microfluidic device that may help evolve the study of parasitic nematodes that are multi-million dollar menaces to the agricultural community.

BIBLIOGRAPHY

1. *Overview and evaluation of fuel ethanol from cellulosic biomass: technology, economics, the environment, and policy.* **Lynd, L. R.** s.l. : Annu. Rev. Energy Environ., 1996, Vol. 21.

2. **Brown, L. R.** Why Ethanol Production Will Drive World Food Prices Even Higher in 2008. *Earth Policy Institute.* [Online] January 24, 2008. [Cited: June 18, 2009.] http://www.earth-policy.org/Updates/2008/Update69.htm.

3. *Environmental, economic, and energetic costs and benefits of biodiesel and ethanol biofuels.* **Hill, J., et al.** 30, s.l. : PNAS, 2006, Vol. 103.

4. *Proliferation response of yeast saccharomyces cerevisiae on electromagnetic field parameters.* **Mehedintu, M. and Berg, H.** s.l. : Bioelectrochemistry and Bioenergetics, 1997, Vol. 43.

5. *Changes in Saccharomyces cerevisiae devlopment induced by magnetic fields.* **Motta, M. A., et al.** s.l. : Biotechnology Progress, 2001, Vol. 17.

6. *Static magnetic fields enhancement of Saccharomyces cerevisiae ethanolic fermentation.* **Motta, M. A., et al.** s.l. : Biotechnology Progress, 2004, Vol. 20.

7. *Yeast cells proliferation on various strong static magnetic fields and temperatures.* **Ostabe, E. S., et al.** s.l. : Journal of Physics: Conference Series, 2009, Vol. 156.

8. *Bioreactor coupled with electromagnetic field generator: effects of extremely low frequency electromagnetic fields on ethanol production by Saccharomyces cerevisiae.* **Perez, V. H., et al.** s.l. : Biotechnology Progress, 2007, Vol. 23.

9. *Static and 50 Hz magnetic fields of 0.35 and 2.45 mT have no effect on the growth of Saccharomyces cerevisiae.* **Ruiz-Gomez, M.J., et al.** s.l. : Bioelectrochemistry, 2004, Vol. 64.

10. *Strong static magnetic field effects on yeast proliferation and distribution.* **Iwasaka, M., et al.** s.l. : Bioelectrochemistry, 2004, Vol. 65.

11. *Selection of high ethanol-yielding saccharomyces.* **Ismail, A. A. and Ali, A. M. M.** s.l. : Folia Microbiology, 1971, Vol. 16.

12. **Dowe, N. and McMillan, J.** *SSF Experimental Protocols - Lignocellulosic Biomass Hydrolosis and Fermentation.* Golden, CO : National Reneweable Energy Laboratory, 2001. NREL/TP-510-42630.

13. *The effect of heat on sugar solutions used for culture media.* **Smith, M. L.** s.l. : Biochemistry Journal, 1932, Vol. 26.

14. **Shuler, M. L. and Kargi, F.** *Bioprocess Engineering: Basic Concepts.* Upper Saddler River : Prentice Hall PTR, 2002.

15. **Sutton, S.** Measurement of Cell Concentration in Suspension by Optical Density. *The Microbiology Network.* [Online] August 2006. [Cited: June 22, 2009.] http://www.microbiol.org/white.papers/WP.OD.htm.

16. *Mechanisms of ageing: public or private?* **Partridge, L. and Gems, D.** s.l. : Nature Reviews Genetics, 2002, Vol. 3.

17. *A new in vitro assay of benzimidazole activity against adult Oesophagostomum dentatum.* **Petersen, M. B., Friis, C. and Bjorn, H.** 11, s.l. : International Journal for Parasitology, 1997, Vol. 27.

18. *Methyridine (2-[2-methoxyethyl]-pyridine]) and levamisole activate different ACh receptor subtypes in nematode parasites: a new lead for levamisole-resistance.* **Martin, R. J., et al.** s.l. : British Journal of Phamacology, 2003, Vol. 140.

19. *Undulatory propulsion.* **Gray, J.** s.l. : Quarterly Journal of Microscopical Science, 1953, Vol. 94.

20. *Artificial dirt: microfluidic substrates for nematode neurobiology and behavior.* **Lockery, S. R., et al.** s.l. : Journal of Neurophysiology, 2008, Vol. 99.

21. *Dissecting a circuit for olfactory behaviour in Caenorhabditis elegans.* **Chalasani, S. H., et al.** s.l. : Nature, 2007, Vol. 450.

22. *Microfluidics for in vivo imaging of neuronal and behavioral activity in Caenorhabditis elegans.* **Chronis, N., Zimmer, M. and Bargmann, C. I.** 9, s.l. : Nature Methods, 2007, Vol. 4.

23. *Oxygen sensation and social feeding mediated by a C. elegans guanylate cyclase homologue.* **Gray, J. M., et al.** s.l. : Nature, 2004, Vol. 430.

24. *Microfluidic devices fabricated in poly(dimethylsiloxane) for biological studies.* **Sia, S. K. and Whitesides, G. M.** s.l. : Electrophoresis, 2003, Vol. 24.

25. NANO SU-8 Negative Tone Photoresist Formulations 2-25. *MicroChem Corp. Web site.* [Online] [Cited: June 24, 2009.] http://www.microchem.com/products/pdf/SU8_2-25.pdf.

26. **Kennedy, M. W. and Harnett, W.** *Parasitic Nematodes: Molecular Biology, Biochemistry, and Immunology.* Wallingford and New York : CABI Publishing, 2001.

27. *The origins and the future of microfluidics.* **Whitesides, G. M.** s.l. : Nature, 2006, Vol. 442.

28. *Trapping the nematode on micro chip for the future of science.* **Zhang, J. X. J.** s.l. : HFSP Journal, 2007, Vol. 1.